Fall 1999

Evaluation of the Transport Properties of GaSb for Bipolar Applications Through Monte Carlo Simulations

Damayanthi Palaniappan
Old Dominion University

EVALUATION OF THE TRANSPORT PROPERTIES OF GaSb FOR BIPOLAR APPLICATIONS THROUGH MONTE CARLO SIMULATIONS

By

Damayanthi Palaniappan
B.E. in Electronics and Communication Engineering
Bharathiar University, Coimbatore, India.

A Thesis Submitted to the Faculty of
Old Dominion University in Partial Fulfillment of the Requirements for the Degree of

MASTER OF SCIENCE

ELECTRICAL ENGINEERING

With an Emphasis on Physical Electronics

OLD DOMINION UNIVERSITY
NOVEMBER 1999

Approved by:

Ravindra P. Joshi (Director)

James F. Leathrum

Linda L. Vahala

ABSTRACT

EVALUATION OF THE TRANSPORT PROPERTIES OF GaSb FOR BIPOLAR APPLICATIONS THROUGH MONTE CARLO SIMULATIONS

Damayanthi Palaniappan
Old Dominion University, 1999
Director: Dr. Ravindra.P. Joshi

GaAs is currently the semiconductor material of choice for high speed, low power applications. Its electronic transport properties are superior to almost all other semiconductors. It is also used in a variety of bipolar applications such as photo-detectors and photo-mixers. However, as is well known, the hole mobility and related transport parameters of GaAs are not very good. This is a serious drawback, and poses a potential problem for all applications involving bipolar conductivity. In order to increase the high frequency limits and high-speed capability of bipolar devices, the choice of an alternative material, therefore, becomes necessary. An important first step towards this goal, would be a theoretical evaluation of the transport properties of other materials, and their comparison with those of GaAs. Here, bulk GaSb is proposed as a possible alternative and an assessment of its electrical response carried out through Monte Carlo simulations.

The main goal of this thesis work is to determine the transport parameters of GaSb for both electrons and holes. Numerical simulation results are obtained for

quantitative evaluation. To facilitate direct comparisons with GaAs and to validate the numerical software, simulations were also carried out for bulk GaAs material. The results obtained have carefully been compared with the available experimental data. An important contribution of this thesis is a demonstration of superior hole transport characteristics in GaSb. The electronic response is also shown to be good under transient conditions. The overall conclusion is a favorable recommendation of GaSb for bipolar applications, and its merit for further studies in actual devices.

Co-Directors of Advisory Committee: Dr. James F. Leathrum

Dr. Linda L.Vahala

ACKNOWLEDGMENTS

This thesis is dedicated to my beloved Parents, brother and sister who gave me the love, strength and encouragement that I needed to take the step towards my Master's Degree.

First and foremost, I would like to thank Dr. Ravindra P. Joshi for having accepted me as his research student. His assistance, guidance and pursuit for perfection served as nourishment for the successful accomplishment of this task. I am very grateful for his patience towards me. It is a great privilege for me to have Dr. James F. Leathrum and Dr. Linda L.Vahala on the defense committee. I appreciate the time and effort they took to critique my thesis work.

Last but not least, I would like to express my sincere love and gratitude to all my friends who supported me and gave me the courage throughout the time I was involved in this program.

TABLE OF CONTENTS

Page

LIST OF TABLES

LIST OF FIGURES

CHAPTER I
INTRODUCTION

1.1 Present Status of Semiconductors

Semiconductor electronic devices have been the mainstay of modern day electronics. Based on semiconductor materials, a wide array of devices are being made for the industrial and military sectors ranging from computer computing, communications and digital processing, to consumer electronics. Though germanium was the first material to be used for semiconductor devices, this was soon replaced by silicon due to its superior properties. Though silicon still enjoys popularity, numerous other materials such as GaAs, InP, SiC and GaN have begun to emerge as the suitable semiconductors of choice for specific applications. For example, the direct bandgap of GaAs and InP make them well suited for opto-electronics. These applications range from photo-detectors to photomixers and optical communications. The electronic transport properties of GaAs are very good, due to its low electronic mass. Consequently, this material finds application in devices such as Field Effect Transistors (FETs) that rely on electronic conduction alone. Similarly, SiC and GaN are emerging as the materials of choice for high-power, high-temperature applications, given their rugged mechanical properties, large breakdown voltage capability, and radiation hardness.

(References in 'Journal of Applied Physics' Format)

There is a constant need for faster device response and to enhance the high speed capability of electronic circuits. Given this need, it becomes increasingly important to search and select the most suitable semiconductor materials for a given application. Traditionally, the industry has stayed with the more familiar set of materials given the knowledge base and processing capability that has already been established over years of research and development. However, if the traditional materials are inherently incapable of meeting ever-increasing demands on the performance limits, it becomes necessary to probe and evaluate other non-traditional materials.

An example is the general class of optoelectronic devices used in photo-detection and sensing of optical signals. These are inherently bipolar devices with both electrons and holes contributing to the overall electrical response. For optimal performance of such devices, it becomes necessary to use a suitable material for which *both* the electron and hole transport properties are very good. Using a semiconductor such as GaAs for which only the electronic transport is superior, but not the hole response characteristics, is insufficient. It, therefore, becomes necessary to evaluate possible alternative materials for a combined optimization of both the electron and hole properties.

Here, bulk GaSb is proposed as a possible alternative semiconductor, and an assessment of its electrical response is carried out through Monte Carlo simulations. The main goal of this thesis work is to determine and establish the transport parameters of GaSb for both electrons and holes. Numerical simulation results are obtained for

quantitative evaluation. To facilitate direct comparisons with GaAs and to validate the numerical software, simulations were also carried out for bulk GaAs material. The suitability of GaSb for high-speed, bipolar applications is gauged in this thesis research.

1.2 Requirements For High Speed Devices

The applications that require high speed and the capability of high-frequency response have some basic requirements that need to be met for ensuring superior performance. A high mobility of both the electrons and holes is one of the vital ingredients. The drift velocity, and transient overshoot characteristics are other useful parameters. These ensure that the device can respond quickly to externally applied signals, and the currents generated will be large. While the former ensures a good frequency response, the latter is useful for maintaining a good signal-to-noise ratio. In addition, suitable device structures need to be fabricated and employed to minimize the circuit effects and external parasitics. The metal-semiconductor-metal (MSM) structure discussed in the next chapter is a typical example in this regard. The MSM has much lower capacitances, is easy to fabricate and lends itself to integration with standard FET technology. Besides, it is possible to scale down the finger spacings and widths of this device for reducing the carrier transit times and the RC time-constants.

One way of evaluating the suitability of high-speed materials is through the direct measurement of the various mobility and velocity parameters. However, this is an expensive and time-consuming task. An alternative to the actual fabrication is numerical simulation studies. Important predictions of the electrical response can be

gauged without costly fabrication. In this thesis, such a numerical evaluation is carried out to determine the suitability of GaSb material for high-speed bipolar applications.

1.3 Outline Of The Thesis Research

The aim of this thesis work is to establish a knowledge-base for the GaSb properties through direct numerical simulations. An additional goal is to carry out direct comparisons with GaAs, which is the material of choice at the present time. The aim is to gauge the suitability of an alternative material such as GaSb for high-speed, bipolar applications. The simulation software used is the Monte Carlo simulation technique. This is a direct and a numerical technique that determines the transient transport characteristics of any semiconductor material. Many of the performance measures like the velocity, kinetic energy of the electron gas, carrier occupancy of the particles and the electron distribution are all evaluated in the simulation. To facilitate direct comparisons with GaAs and to validate the numerical software, simulations were also carried out for bulk GaAs material. The results obtained have carefully been compared with the available experimental data. An important contribution of this thesis is a demonstration of superior hole transport characteristics in GaSb. The electronic response is also shown to be good under transient conditions.

The contents of the following chapters are described next in a brief summary form. Chapter 2 comprises an overview of the research work that has already been done in this field. This chapter basically provides a literature review and forms the background for this thesis work. Previous work on photo-mixing is discussed in this

chapter since it is a typical high-speed application involving bipolar transport. The general principle behind the process of photo-mixing is explained, and the importance of material characteristics for obtaining high-speed is brought out. This is followed by a discussion of the material properties of GaAs and GaSb. The values of the various known parameters are listed in order for a comparison. The modeling technique used here, which is the Monte Carlo simulation, is then briefly mentioned in the later part of this chapter.

In chapter 3, the Monte Carlo simulation procedure is presented in a more detailed manner. The flowchart of the basic procedure is given and the method by which it is applied to particle transport is clearly stated. The various scattering mechanisms that exist in the process of carrier transport are discussed, though all of them are not accounted for in the simulation. This presentation brings out the complexity of the simulation chosen, and is aimed to stress its accuracy. Next, a validation of the Monte Carlo numerical implementation is presented through careful comparisons of the transport predictions for GaAs with published data. GaAs has been chosen since its transport properties are well documented, and also because it is the reference material for baseline comparisons. Results such as the field-dependent transient velocities, kinetic energy of the mobile carriers, ratio of electron populations in the various valleys, and distribution function of the electrons were obtained. Good agreement with published GaAs data demonstrates the validity of the present numerical implementation.

Chapter 4 presents the results of this research work with accompanying discussions. The simulation is carried out in order to ascertain the mobility of holes in GaSb, and to obtain comparisons with the GaSb material. The various results obtained are given in this chapter. The simulation results of GaSb mobility and drift velocities for both the holes and electrons are given. The results clearly demonstrate that the steady state characteristics of holes are better for GaSb as compared to those of GaAs.

Chapter 5 presents the concluding summary for the whole thesis work. This chapter summarizes the main accomplishment and contributions. The primary conclusion in favor of using GaSb for high-speed, bipolar transport is presented. Finally, the scope for future work that could be carried out to utilize the advantages of the GaSb material has been listed. This would serve as the key for extended follow-up work in this area.

CHAPTER II

BACKGROUND AND LITERATURE REVIEW

2.1 Introduction

In this chapter, the primary objectives of the thesis research are presented and discussed. Appropriate background material is given, in conjunction with a brief review of the related issues and open questions in this general area. Essentially, the central goal is to carry out a detailed evaluation of the suitability of GaSb, which is a relatively unexplored material, for high speed, bipolar applications. The GaAs semiconductor has already been explored by many researchers and finds applications in many electronic devices and components. However, due to the low mobility of mobile holes in GaAs, this material is perhaps not the optimal semiconductor of choice for bipolar applications. As a practical and inexpensive first step in trying to ascertain the viability of the GaSb material, numerical calculations of the expected electrical transport characteristics are perhaps the best option. Such an evaluation and theoretical simulation study has been carried out here through appropriate Monte Carlo-based software in the present thesis.

As background to the possible utility of the new GaSb material, some of the high speed bipolar applications are highlighted and discussed in this chapter. Previous work related to these areas is also presented. Optical heterodyning, optical detection of signals in the terahertz range, and the capability of a broadband radiation emitter are some of the applications in this regard. These have been discussed, and a brief background of hetero-dyning used in the context of photo-mixing in semiconductors is also presented. A summary of the reported data on different photo heterodyne devices relevant to this objective is also given. Next, some of the modeling and simulation aspects appropriate to the current high-frequency evaluation problem are also discussed at the end of this chapter. This chapter thus presents a general background and

overview, lists previous work, and establishes the research issues which are subsequently taken up in the following chapters.

2.2 Central Objective

The main aim and scope of this project is the numerical evaluation of the viability of GaSb for high-speed device fabrication. This is accomplished through simulations of the electrical transport characteristics due to the electron-hole plasma within the bulk semiconductor material. The material has been chosen as a result of several considerations which include: the high field capabilities, effective masses of both the electrons and holes, free carrier mobilities, and the ease of fabrication of the material. Some of the relevant properties of GaSb have, therefore, been presented and discussed in this chapter to provide a suitable background. The GaSb material is chosen for the high-speed bipolar applications, due to a variety of advantages it provides as mentioned in the later part of this chapter. The particle based Monte Carlo scheme is employed here for simulation purposes, and is given in detail in the next chapter. The technique is very accurate, though computationally intensive, and provides a clear description of the electrical performance, under both steady state and transient operating conditions. The accuracy and validity check of the present simulations is carried out through careful comparisons between the numerical predictions and existing data on the transport properties of the well-known GaAs material. Some of the past work, especially with regards to optical heterodyning concepts for high-speed optoelectronics is discussed next, in the following section.

2.3 Background and Past Work On Semiconductor Based Photo-Mixing

Photodetectors cannot, in general, process phase related information but are only responsive to them. However, through the process of optical "heterodyning" or "photo-mixing," measurements of both the amplitude and phase of the optical signals can be accomplished. This idea is very similar to the principle of super heterodyne receivers in the context of microwave and radio-frequency detectors, for which the mixing is done with the help of a local oscillator. From the experimental background and previous reports, it seems that the photo mixing technique can also be used as a means for coherent micro- and milli-meter wave generation [1]. It was discovered that the output power of these optical heterodyners and their reproducible device structures could be improved by means of semiconductor devices like GaAs.

This process involves the incidence of two electromagnetic signals on a direct band gap semiconductor material such as GaAs. As a result, internal photo currents are produced upon the application of an external bias [1]. These photo currents produced are due to the motion of charges following photo-generation of electron hole pairs within the device. If high carrier mobility were to be exhibited by the chosen semiconductor material, then the photocurrents would be large. Also, the rise time would be very short. Hence, the choice and selection between various semiconductor materials becomes critical for achieving speed and signal magnitude in photodetectors. Using a material with better transport properties will result in faster response with a higher magnitude. The movements of the electrons and holes are in the opposite direction, but they provide unidirectional current due to the difference in their charge polarity. This current, which represents the conversion of optical energy to electrical signal, can be used for detection.

The photo-generated carriers can also be made to undergo large accelerations either by applying a high bias or by using the built-in surface electric fields. This can lead to the production of a coherent radiative output, as the accelerating charges act as a source term for generating time varying electrical and magnetic fields as given by the Maxwell equations. For either application, (i.e. the detection or coherent radiation), the advantage of this process is its inherent simplicity and lack of complex external biasing circuitry.

2.3.1 Results Of MSM Photo Detectors:

Metal-semiconductor-metal photo devices with picosecond temporal response for photomixer applications around 830 nm have been successfully fabricated and tested [2]. Metal semiconductor metal (MSM) photodetectors have become popular in optoelectronic communication systems, chip inter-connects and high speed sampling applications. This is due to a variety of advantages for the MSM system which are worth noting. These benefits include : large bandwidth, low voltage operation, smaller device capacitances per unit area, low leakage currents and compatibility with planar field effect transistor technology. The MSM devices generally have improved speed and frequency response due to the use of low temperature GaAs material which enhances bulk recombination and allows higher breakdown fields; the use of nanoscale separation between the metallic finger, which helps reduce the carrier time and enhances the possibility of ballistic transport; and the reduction in finger widths which effectively lowers the device capacitance. Having known the optical detection capability of a MSM, the device can be used as a photomixer element in a submillimeter detection system. An ultra fast high frequency photomixer has been tested, and its electrical response based on the use of nanoscale, LT GaAs based MSM devices having narrow finger widths was analyzed [2]. The

transient response was measured at a wavelength of 830 nm, 150fs FWHM (frequency width for half maximum) laser excitation. The experimental results were carefully compared with the predictions of a comprehensive, bipolar, two-dimensional Monte Carlo simulator which included circuit loading effects. The experimental values were obtained from an electro optic sampling system through an electro optic sampling system as desired. The MSM photodetectors consisted of a planar multifinger inter digitated electrode formed by depositing gold titanium (Au/Ti) schottky contacts over the optically active layer. A thick AlGaAs layer was necessary surface passivation and lays on top of a LT GaAs optically absorbing layer. In order to facilitate impulse response testing, the devices were embedded with a coplanar transmission line. A bipolar Monte Carlo code was used for all the numerical simulations. The electron and hole parameters for GaAs were the same and the data for AlGaAs were obtained from an extrapolation between the GaAs and AlAs parameters. Some of the electrical properties of GaAs at 300 K are summarized below in table 1. Ionized impurity scattering, polar optical transitions, intervalley deformation potential mechanism, and interactions with the acoustic phonon modes were all taken into account. Alloy scattering was additionally included for AlGaAs layer. The two dimensional electric fields were continually obtained after every time step of the Monte Carlo simulation from a Poisson Solver. In order to facilitate the carrier transport, absorbing boundary conditions were used for the bottom surface and the top contacts, and total carrier reflection was used at all other boundaries to account for periodic injection from the neighboring cell of an actual MSM repetitive structure.

The MSM response was measured and simulated at a very high wavelength in the order of 800nm. A higher wavelength had the advantage of a lower internal device heating due to lower photon energy. The transient velocity overshoot was much higher for optical excitation near

the band edge. The calculations for this nanoscale device included the details of optical pulse and scattering rates dependent on energy. The response at longer times was strongly affected by holes and lower energy electrons that remain in the device within regions of relatively low electric field.

Effective Density of States Valence Band N_v cm^{-3} Conduction Band N_c cm^{-3}	 7×10^{18} 4.7×10^{17}
Energy Gap, eV	1.43
Melting Point (K)	1513
Intrinsic mobility of electrons(cm^2 /V-s)	8600
Intrinsic mobility of holes(cm^2 /V-s)	400
Thermal Conductivity(W/cm- ^oC)	0.46
Crystal Structure	Zinc Blend
Effective electron mass	0.063
Effective hole mass	0.05
Breakdown Field (V/cm)	4×10^5

Table 1 Electrical Characteristics of GaAs

The two-dimensional Monte Carlo model provided very accurate predictions of the transient MSM response. The results suggested that the inability of the electric fields to penetrate deep into the

active areas might limit the frequency response to the nanoscale devices. Also, the low mobility of holes in GaAs slows down the overall response of this bipolar device. Finally, on the basis of this previously reported work, it is clear that the Monte Carlo simulation technique is a suitable tool for simulating transport and electrical properties of semiconductors.

2.4 Overview of GaSb Material Properties

The band structure of a three-valley semiconductor is shown as in figure 2.1. The electrons initially reside in the main valley of the conduction band. The transport features resulting from

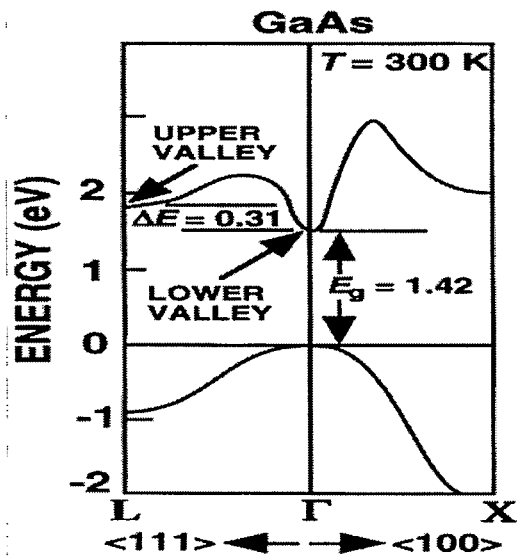

Figure 2.1 Band diagram of a three valley semiconductor material GaAs

such a 3-valley bandstructure are briefly discussed next. When an external electric field is applied, the electrons acquire energy, and move to higher states in the lowest Γ–valley. However, most of them still remain in the lowest valley if the field is less than a certain threshold value. On the other hand, if the electrons were to acquire even more energy, many of them would be scattered into the upper valleys. A higher effective mass in the upper valley reduces the mobility,

and so the average drift velocity automatically decreases. At larger energies, i.e. at higher electric fields, most of the electrons are transferred to the upper valley where they have higher effective mass and a lower mobility. If the electric field is increased still further, the drift velocity eventually begins to increase due to the higher accelerating force provided by the external battery. If, on the other hand, the electric field is lowered below the threshold value, then the electrons gradually begin to lose energy and are eventually scattered back to the main Γ-valley. This is the situation for GaAs, and is expected to occur for the GaSb material as well since it also has a multi-valley conduction band.

Gallium Antimonide and related compounds have begun to generate a great deal of interest for a range of electronic and optical applications in recent years[3,4]. The growth of GaSb

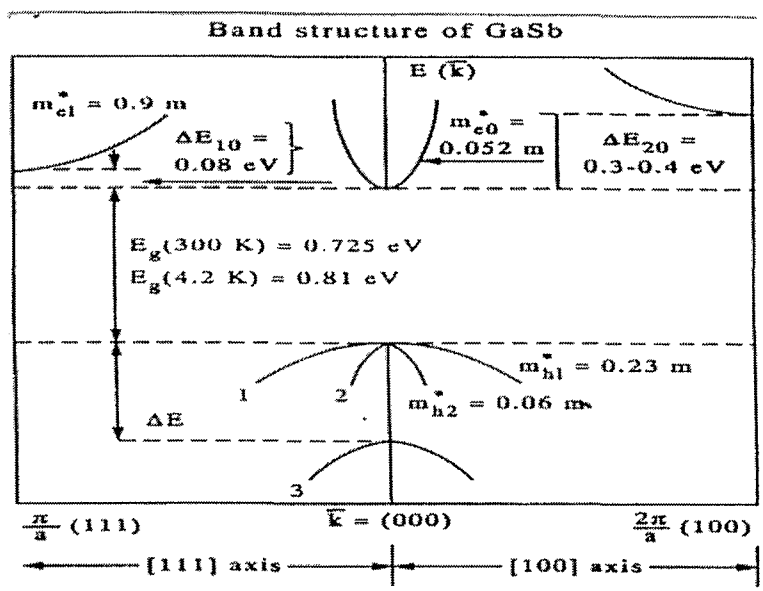

Figure 2.2 Energy band diagram of GaSb.

by Metal-Organic Chemical Vapor Deposition [5] and Molecular Beam Epitaxy(MBE) [6] has led to the development of resonant tunneling devices[7], infra red lasers[8], photodiodes[9], wavelength infrared detectors[10], electro-optic modulators[11] and second harmonic generators[12]. The energy band diagram of GaSb is shown as in figure 2.2 . GaSb has a band gap 0.72 ev at room temperature and a cubic lattice constant that is appreciably larger than for GaAs [3]. GaSb has a melting point which is lower than that of GaAs, but it is more stable against oxidation by water-vapor unlike some compounds with a high Al content. Undoped GaSb that is bulk grown is usually the p-type in character, with a hole concentration on the order of 10^{16} cm^{-3} . Some of the electrical and other properties of GaSb that are known and others that have been used for the simulations carried out in this thesis work are presented in table 2 given below.

GaSb is a direct band gap material and so of interest for optical devices. An important feature of GaSb is that the L-Valley lies only about 85mev above the Γ valley. Hence is it barely qualifies as a direct band gap semiconductor. It therefore becomes very easy for the material to be converted into an indirect band structure either by applying suitably large magnetic fields[13], static pressure[14], or through novel quantization [15]. The L-band of GaSb has an ellipsoidal constant-energy surface and so it allows inter sub band transitions. This feature opens up possibilities for long wavelength optical detection. Another advantage of GaSb is that it provides for type II band alignment in super lattices and quantum wells when used in conjunction with the InAs system. These structures are recognized as promising candidates for mid infra red lasers due to the inherent suppression of internal electron hole recombination.

Despite the emerging technological importance of GaSb, there are not many reports that describe its bulk electronic properties in detail. However, electronic mobility was calculated as a function of temperature for high purity GaSb , with only the Γ valley considered. Though the band gap is direct, but the L-valley is only 80-85 meV above the Γ-band minimum. Some data is available on the barrier heights of GaSb metal contacts. For example, studies of Schottky barriers were performed in which the GaSb surfaces were chemically etched with dilute Bromium in Methanol prior to metal deposition of the contact. Capacitance voltage measurements at 300 K yielded barrier heights of 0.5 eV for Ga and 0.42 eV for Sb. The Fermi level at the surface tended to be pinned slightly above the valence band edge and the barrier height was not directly related to the metal work function. When the temperature decreases the GaSb band gap increased with an increase in the barrier height, indicating that the Fermi level tends to track the valence band edge. Also, generation recombination currents from a near midgap center were shown to dominate the ideality factors, as expected since the barrier heights were significantly greater than half the GaSb bandgap.

The electron mobilities were measured to be in the 4000-5000 cm^2 /V-s range in bulk GaSb at 300K. This is quite comparable to the electron mobilities of GaAs , for which the graphs are shown later in chapter 3. The hole mobility is expected to be as high as that for GaAs, if not better.

Γ-valley effective mass	0.042
L- valley longitudinal effective mass	1.40
L –valley transverse effective mass	0.085
X-valley longitudinal effective mass	1.3
X-valley transverse effective mass	0.75
Density (g/cm^3)	5.613
Γ-valley non parabolicity (eV^{-1})	0.4
L-valley non parabolicity(eV^{-1})	0.27
Relative permittivity(High frequency)	14.44
Relative permittivity (Static)	15.69
Longitudinal elastic constant(dyn/cm^2)	$1.04x10^{12}$
Transverse elastic constant(dyn/cm^2)	$3.55x10^{11}$
Acoustic deformation potential(eV)	9.3
Γ-L valley separation(meV)	84.7
Γ-X valley separation(meV)	325
Polar optical phonon energy(meV)	29.7
Effective intervalley phonon energy(meV)	23.76
Γ-L intervalley deformation potential ($eV\ m^{-1}$)	$6x10^{10}$
L-L intervalley deformation potential ($eV\ m^{-1}$)	$5.7x10^{10}$
L-X and X-X intervalley deformation Potential($eV\ m^{-1}$)	$1.0x10^{11}$
Heavy hole effective mass	0.28
Light hole effective mass	0.05
Warping parameters(A,B,C)	11,6,11
Average sound velocity(cm/sec)	$3.24x10^5$
Non polar optical deformation potential(eV)	6.1
Transverse optical phonon energy(meV)	27.4
Breakdown field	$5x10^4$
Mobility of electrons (sq.cm /v/s)	3000
Mobility of holes (sq.cm /v/s)	1000
Diffusion coefficient of electrons (sq.cm/s)	75
Diffusion co efficient of holes (sq.cm/s)	25
Electron thermal velocity(m/s)	$5x10^5$
Hole Thermal velocity (m/s)	$2.1x10^5$

Table 2 Parameters used for the particle simulation of GaSb

2.4.1 GaSb Simulation Parameters

In this thesis, a three-valley model has been used, and anisotropy effects included by explicitly incorporating all equivalent L and X valleys. Most of the material parameters have been chosen from the literature [3,16]. However, effective mass values have been taken into account here from the recent cyclotron resonance data of Arimoto et al, while the Γ-L valley deformation potential was set to $6x10^{10}$ eV cm^{-1} in keeping with recent pump probe experimental data [17]. Data on the wavelength dependent effective masses was used to extract the non parabolicity [13]. Inter valley scattering was chosen using a single effective deformation potential, assumed to take account of the various symmetry allowed phonon processes. The model included electron intravalley interactions with acoustic nodes via the deformation potential, polar optical phonon processes, and impurity ion scattering.

The results, as will be presented and discussed in Chapter 4, obtained on the basis of the above material parameters yielded good results for GaSb. These graphs are shown in chapter 4. At 300K, the hall and drift mobilities are essentially the same over a large carrier concentration. Ionized impurity scattering has been shown to be quite important and would limit the response at low temperatures. The results, given in chapter 4, show that the transient drift velocities can be higher than the corresponding values for GaAs. This arises from the fact the Γ valley effective mass is lower in GaSb. This makes it more suitable for high speed optical detectors.

2.5 Modeling Techniques

The modeling approach used for the simulation is the stochastic-kinetic Monte Carlo technique. The modeling is carried out for performing numerical simulations, in order to obtain a

better understanding of the underlying physics and the device performance. The Monte Carlo Method adopted provides a more accurate and direct analysis of ultra fast transient phenomena inside the semiconductor. It was chosen for the accuracy, and its previous success in predicting the response of GaAs MSM photodetectors. The technique also allows the inclusion of several effects due to high electric fields and small dimensions, which is an important advantage. The Monte Carlo simulation, in this case, simulates the particle motion (holes and electrons) at every time step. It keeps track of all the scattering processes encountered by the particles inside the semiconductor. The simulation is carried out for the semiconductor material GaSb using the parameters in table 2 as above and the method is verified by the comparison of these results with the ones already obtained for GaAs material. They are presented in chapter 4.

Modeling seems to be advantageous for a variety of reasons. It is inexpensive, quick, and yields a feasibility study. The geometrical parameters can be easily changed and repetitive simulations can be carried out with ease, till the relevant and appropriate results are achieved. Various structures and operating conditions can be simulated easily and rapidly.

CHAPTER III

THE MONTE CARLO SIMULATION TECHNIQUE

3.1 Introduction

The study of carrier transport in semiconductors and the details of its various physical mechanisms have become very important for gauging the effectiveness and utility of electronic devices. Determination of device performance levels for a variety of applications is often made on the basis of simulation predictions. In order to attain realistic simulations and physically accurate results, one needs to ensure two aspects. First, valid semiconductor models must be employed. Second the simulation schemes must be of high accuracy and precision. Typical issues of interest with regard to the semiconductor model include details of the semiconductor band structure, impact ionization coefficients, carrier lifetimes, deformation potentials, carrier effective masses, phonon frequencies, and other material parameters. Most of these need to be obtained through experimental measurements as discussed by Schroder [20]. The experimental techniques include Raman spectroscopy [21], cyclotron resonance [22], deep level transient spectroscopy [23], and so on. Fortunately, most of the materials of common interest to the semiconductor industry have been studied and the parameter values reported in the literature [16]. Charge transport in semiconductors is in general, a tough problem due to the non-linearity of the response and complications arising from the complex device geometry. Though several simulation methods exist and have been used to predict the transport response, most of them are not very accurate, and can only be applied under specific conditions. For example, the simplest is the drift-diffusion scheme

[24]. It can be derived from the Boltzmann equation [25] with several approximations. For instance, it ignores the distribution functions that characterize carriers in velocity and real space within semiconductors. Instead, averaged carrier densities are used.

The governing Drift-Diffusion equation is given as:

$$J=nqV_n+pqV_p - qD_n \nabla_n+qD_p\nabla_p \quad (3.1)$$

where J is the current density, n and p are the electron and hole densities, D_n and D_p are the electron and hole diffusion coefficients, v_n and v_p are the electron and hole drift velocities and q is the electronic charge. This equation is derived from the Boltzmann transport equation under the following assumptions:

a) An isotropic and parabolic single band.

b) Inherent assumption of the relaxation time approximation.

c) Absence of degeneracy with no hot carrier effects.

d) Homogeneous collision time. For example, a single energy-independent relaxation time is assumed for mobility calculations. The validity of the drift-diffusion scheme also requires that the scattering time be significantly smaller then the simulation time scale of interest.

e) No strong off-equilibrium effects, and

f) An assumption that the length scales for spatial variation of the electric field and impurity concentrations are much longer than the carrier mean free path.

In the Boltzmann transport approach, which represents a higher level of sophistication, a governing integro-differential equation is obtained for the equation of motion for the distribution function f(r,p,t) of the particle ensemble [25]. This distribution function

f(r,p,t) is the probability of finding a particle with momentum p at a position r at time t. The Boltzmann Transport Equation (BTE) incorporates all of the internal scattering effects taking place over time, and is thus able to describe non-equilibrium, transient effects correctly, provided the scattering relationship can be characterized. Usually, time-dependent perturbation theory based on the Fermi Golden rule is used to ascertain the scattering relationships. However, the Boltzmann transport approach is usually restricted to inherent assumptions, such as a simplified treatment of the band structure and distribution functions. This approach fails in cases where simplified distribution does not exist, such as in very short dimensional structure or during ultrashort transient time intervals.

In order to correctly simulate semiconductor structures having very small dimensions, for phenomena involving ultrashort time scales, or when the assumptions of the BTE become unacceptable, another approach called the Monte Carlo Approach is used for greater accuracy [26,27]. In the stochastic Monte Carlo approach, individual particles are randomly selected and their motion followed in space and time. The average ensemble behavior is subsequently determined by collecting enough information about the particles. The biggest advantage of this method is that, no fitting parameter is required. However, the approach is very intensive computationally since a large number of particles are required for simulation.

The Monte Carlo method is the most popular and accurate of the semi-classical techniques that have been proposed thus far. Given its accuracy and inherent merits, it will be used here for transport simulations in this research work. In this kinetic scheme, the motion of individual particles within a semiconductor is tracked. The Monte Carlo

simulation offers an alternative approach to analytical techniques, and is based on concepts of statistical sampling of the distribution functions of random processes. The main principle behind the Monte Carlo simulation is that motion of charged particles is monitored based on Newtonian mechanics over discrete time steps. The random nature of the scattering processes is simulated based on the assignment of random numbers. The principle disadvantage and drawback of this Monte Carlo scheme is the computational intensity and long execution times.

The Monte Carlo simulation provides a solution to particle transport and facilitates the evaluation of specific quantities of interest such as carrier drift velocities, electron mobility and kinetic energies, carrier distribution functions in phase space, noise power and spectral density. A unique feature in solving transport problems by Monte Carlo is that the individual particle histories are simulated [28,29]. This method proves to be very efficient and useful as it allows for the prediction of microscopic phenomena that cannot be separately observed in experiments and the investigation of materials whose parameters are not well known. This technique is easy to implement and offers the following advantages:

1) The microscopic interpretation of the physical details is quite transparent.
2) Stochastic calculation is achieved at a minimum level of difficulty while incorporating memory effects.
3) Temperature gradients and fields (both electric and magnetic) can all be comprehensively included.
4) Time and space dependent phenomena can be easily simulated.
5) No arbitrary assumption regarding the distribution function needs to be made.

6) Easily includes system memory effects and hence all non-Markovian behavior.

7) Arbitrary shapes and geometries, as well as complicated boundary conditions can be analyzed with ease.

Monte Carlo is a statistical numerical method used for solving mathematical problems. It was born well before its application to the transport problems, and has been applied to a number of scientific fields. In the case of charge transport, the Monte Carlo turns out to provide a valid solution to the Boltzmann equation. This method was first applied to transport in semiconductors by Kurosawa [30] to study steady-state hole transport in Ge through the inclusion of a "self-scattering" scheme. Fawcett et al. [27] extended this method for use in GaAs where different scattering processes and band structures were incorporated. Details of the technique are given in the following sections.

3.2 Basic Principle

The Monte Carlo method, as mentioned above, relies on the random number generation to model the random processes associated with transport and internal scattering. The random samples are usually computer generated by a variety of algorithms. The easiest way for computer generation is based on the idea of "pseudo random" sequences produced by standard arithmetic subroutines. In the present research work, the Monte Carlo (MC) simulation algorithm written in the Fortran software language uses one of the built-in pseudo-random library routines. The movement of a large number of particles (10,000 in this research) is then tracked based on Newton's laws of motion. The driving forces can be due to electric fields, magnetic forces or

thermal gradients, and can be specified based on the precise conditions of a given problem. This is thus a kinetic approach based on a "billiard-ball" representation of the charged particles. The drift velocity, kinetic energy, momentum, and population of particles in each of the valleys are then calculated at regular time intervals. This yields statistically representative information on the transport of particles in the actual semiconductor. In the beginning, the initial velocity and energy of the particle ensemble need to be provided as the inputs. The motion of the charged carriers is peppered by discrete collisions, also known as scattering events. These collisions are stochastic in nature, and arise due to the interactions with phonons (lattice vibrations), surface roughness or ionized impurities. The Monte Carlo method selects the type of scattering mechanism, and final state based on energy dependent probabilities. Random numbers are used to map these probabilities to actual values in a stochastic fashion.

3.3 The Monte Carlo Simulation Technique

3.3.1 The Basic Monte Carlo Method

The first stage of the simulation starts with the description of the physical system. This means, defining the parameters of the physical system, assigning their values and providing the geometry. Some of these parameters include: the initial carrier energy and momenta, starting positions, duration of the simulation, and valley occupancy index. The particles are assumed to have initial velocities and are considered to be moving unimpeded until they encounter a physical perturbation such as a phonon, or collision with other carriers or imperfections. At the time of free flight, the external forces are made to act according to the relation :

$$\hbar\,[dk/dt] = qE \quad (3.2),$$

where 'k' is the carrier wave vector , 'q' is the charge and $\hbar = h/2\Pi$, 'h' being Planck's constant. Quantities such as the carrier velocity, energy, etc., are all computed and updated during this stage. Each free flight stage ends with a collision, with the free flight time duration being a random variable. The second stage of simulation is the choice and selection of a particular scattering mechanism according to the probabilities of each individual process. The scattering rates for each mechanism are typically energy dependent. Hence, a "scattering rate table" which serves as a simple look-up chart is computed prior to the start of the transport simulations. This scattering rate table computation is thus done within the program code immediately following the parameter initialization. In the second stage, the scattering mechanism is selected. The energy and momentum values of the scattered particle are then adjusted in accordance with the type of scattering process chosen. For example, an elastic process does not change the energy, while inelastic scattering warrants the increase or decrease of the energy. The values calculated at this point serve as the starting values for the next free flight stage. Thus, the entire process is replicated until the desired end of the simulation run. The conventional way to evaluate at the precision of this scheme is to carry out parameter determinations at a large number of time intervals and average over the different values. The large number of particles and the repeated determination at various times serves to suppress the statistical uncertainty. Standard deviation of the estimators can in principle, be used to reveal the accuracy.

3.3.2 Technique Details and Scattering Mechanisms

In the first part of the program, the material parameters and values of all the physical quantities such as the operating temperature, applied electric field 'E', doping density, time step and total simulation time, initial carrier energies and momentum, etc., are set to the desired values. The material parameters such as the coupling strengths describing the particle interactions with the lattice, effective masses, phonon energies and band structure are also provided. The next issue in the calculation would be to determine the time of free flight and choose a scattering mechanism using the probabilities contained the scattering rate table. The free flight duration and the scattering mechanism go hand in hand, as one dictates the frequency of the other. The free flight is disturbed only by a potential perturbation. Therefore, its duration can be computed if the scattering rate is known. Based on the perturbation concept, the scattering rate is calculated with the knowledge of the perturbing potential. For a process of scattering from an initial state k to a final state k', this can be expressed as :

$$\lambda(k) = \Sigma\lambda_n(k) = \Sigma \int_{n=1}^{N} S_n(k,k')dk' \qquad (3.3) \ ,$$

where S(k,k') is the transition rate from state k to state k', 'n' is the index for the nth individual scattering process, the 'Σ' 1 to N denotes a summation over all the possible 'N' processes, and λ(k) defines the total transition rate for a particle in state 'k'. Hence, the probability that a particle has suffered a collision at time t = 0 and has not yet suffered another collision until the time 't' is denoted as,

$$\exp\left(-\int_0^t \lambda(k(t')\,dt')\right) \ .$$

Also, the probability of next collision during time interval dt around t will be then be

given by :

$$P(t)dt = \lambda(k(t)).\ \exp(-\int_0^t \lambda\ (k(t')\ dt')\ dt \qquad (3.4).$$

Since every particle must undergo a scattering process sooner or later, one obtains :

$$\int_0^\infty P(t)dt = 1 \qquad (3.5).$$

In order to resolve this complex distribution, it is mapped on to a pseudo random distribution with known probabilities, p(q) for the physical distribution and p(r) for the pseudo random distribution as,

$$(\int_a^q p(q')\ dq'\ ) / (\int_a^b p(q')dq' = \int_0^r p(r')\ dr' \qquad (3.6).$$

This mapping relation is associated with a uniform distribution, as it is readily available in all the computer systems. In the above equation, 'a' and 'b' represent the maximum and minimum value for the physical distribution parameter 'q'. We know that for the uniform distribution, the total probability on the left side equals unity. Therefore,

$$p(r)=1 \quad \text{and} \quad r = \int_a^q p(q')dq' / \int_a^b p(q')\ dq' \qquad (3.7).$$

The equations above implies that to obtain the time, t, at which a scattering event occur, one could generate a random number "r" between 0 and 1 such that the following equality would hold :

$$r = 1\text{-}\exp(-\int_0^t \lambda[k(t')dt'] \qquad (3.8\ ).$$

Though accurate, the above form does not lend itself to a straightforward evaluation. This occurs because the scattering rate λ (k) is not a constant. The integral, thus, needs to

be evaluated numerically. This can become almost intractable as the numerical integration would have to be performed for a given r and t for each value of 'k' in order to solve for the time variable. In order to overcome this difficulty, a mechanism first devised by Rees [31] that introduces a new fictitious 'self scattering' mechanism is typically used. This addition of a self-scattering mechanism allows the total scattering rate $\lambda(k(t))$ to be a constant ($=\Gamma$), and thus simplifies the above equation to :

$$r=1-\exp(-\Gamma t) \qquad (3.9)\,.$$

The total scattering probability now becomes $\lambda_T(k)=\lambda(k)+\lambda_v(k)=\Gamma$ due to the fictitious self scattering. As the name implies, the self-scattering mechanism does not produce any tangible effect on the state of the particle. Since it is not really a scattering process, the new state of the electron after undergoing the self-scattering process is made to remain unchanged. Thus, the electron continues to be moving in its own free flight condition without having been disturbed by at all. The collision velocity is assumed to be a constant and the time at which the scattering occurs is calculated as:

$$t= -\,1/\Gamma \ln(1-r) \qquad (3.10).$$

The random numbers 'r' are evenly distributed between 0 and 1 , and so 'r' and '1-r' both have the same physical meaning. This changes the equation to :

$$t= -\,1/\Gamma \ln(r) \qquad (3.11).$$

This result allows for a simple determination of the flight time by means of a uniform distribution of the random numbers "r". This ends the first stage of the MC process. The flowchart of a typical Monte Carlo simulation is depicted in the figure (fig 3.1) below.

In the second stage of the process, the particle is assumed to be moving freely under the influence of the applied electric field. It obeys Newton's laws of motion. The particle

when disturbed by a perturbation during its free flight, then scatters and the next free flight time 't' is calculated as outlined in the first stage. Important carrier parameters such as momentum and the energy are recorded for obtaining the averaged macroscopic values.

The selection of precise scattering mechanism at the end of the free flight time for each particle is the next important step. The scattering rates for the various mechanisms are calculated as a function of the carrier energy and normalized to unity upon a division by the maximum total value scattering rate 'Γ' . This value 'Γ' is the maximum sum over all the energy dependent processes. This means that for a given energy 'E' the normalized probability for the i th scattering mechanism is represented as $P_i(E)/\Gamma$.

The choice of the actual scattering mechanism is fairly straightforward, and is based on the above normalized probability $P_i(E)/\Gamma$. It is obtained by generating another random number r between 0 and 1. Based on this random number, the j th scattering process would be chosen on the basis of the following inequality :

$$\sum_{i=1}^{i=j-1} P_i(E) < r < \sum_{i=1}^{i=j} P_i(E) \qquad (3.12)\,.$$

However, in case 'r' was greater than the sum of the probabilities of the total number of actual scattering mechanisms, then the self-scattering process would be chosen. This overall selection scheme is shown later in this chapter. After the selection of the scattering mechanism, the simulation proceeds on to calculate the next free flight time. The new state k' of the particle following scattering has to be evaluated next. If a self-scattering mechanism has been chosen, the new state is set to exactly equal the value before scattering. On the other hand, if the selection results in a real scattering mechanism, then the new state is chosen stochastically in accordance with the detailed

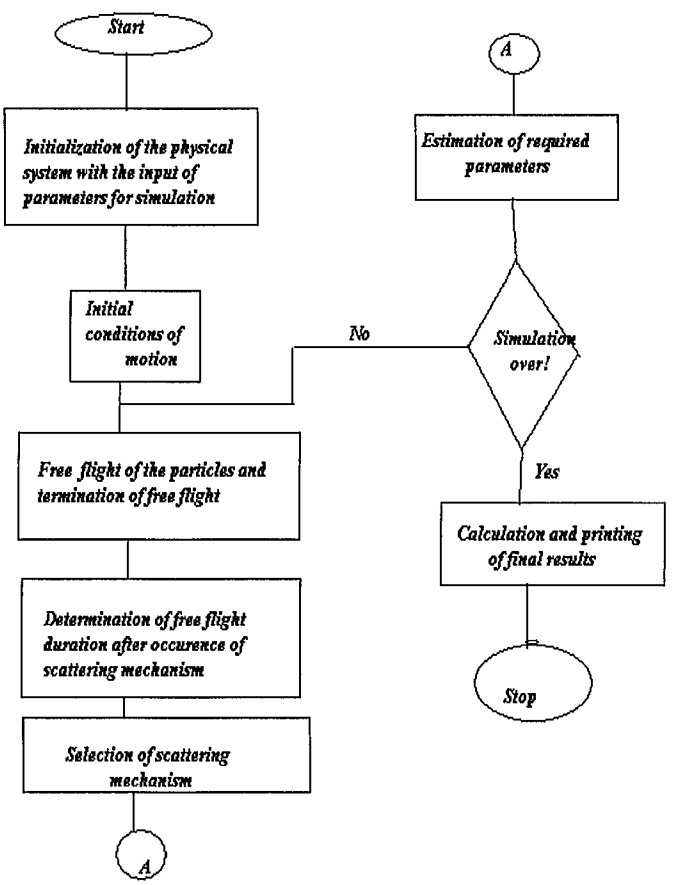

Figure 3.1 Flowchart depicting a typical Monte Carlo Simulation

characteristics of the particular scattering mechanism chosen. Details of some possible scattering mechanisms used in this research are given in a later section.

3.4 Scattering of Charge Carriers

Scattering is a general term for the interaction of the carrier with the surroundings. The various scattering mechanisms could be classified in a very broad manner and is depicted in the chart shown in Fig. 3.2. An electron in the crystal, under the influence of an external force, such as an electric field, picks up energy during its acceleration. However, this energy and momentum is changed by scattering that comes about because of lattice vibrations or changes in potential due to impurities and defects or the presence of ionized donor/acceptor charges. The particle undergoes a transition from its initial state to a final state as a result of a scattering process. If the transition

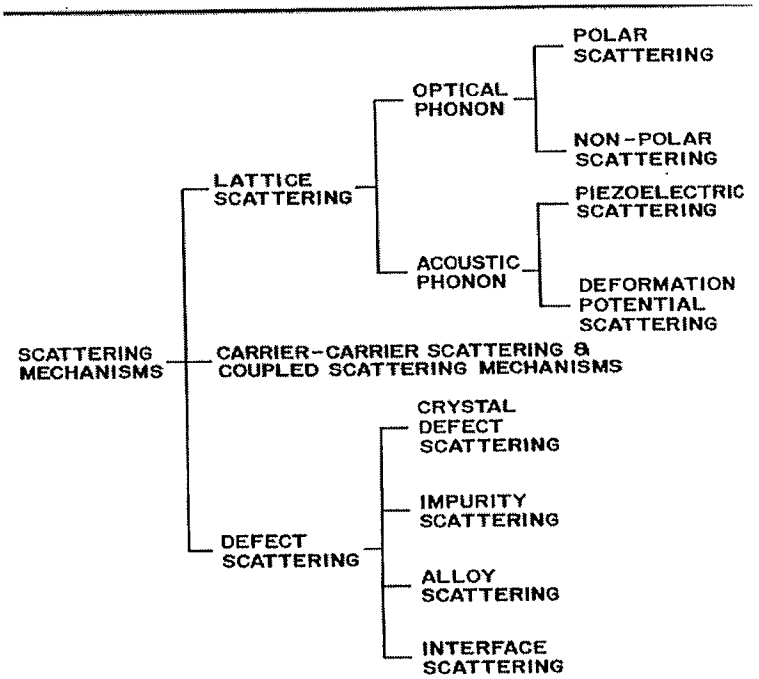

Figure 3.2 Schematic of the various scattering mechanisms based on their origin

involves two valleys it is called as inter valley transition. Otherwise, it is intra valley scattering. In this thesis, all of the important scattering mechanisms such as polar optical scattering, non -polar optical scattering, non-equivalent and equivalent inter valley interactions, piezoelectric, acoustic and ionized impurity processes have been considered.

The role and magnitude of the various scattering mechanisms could be visualized by a graph of the scattering rate versus energy. The energy dependent scattering rate is calculated for different mechanisms from the computer simulation program for the GaAs material, and is shown in Figures. 3.3,3.4 and 3.5 for the Γ,L and X valleys respectively.

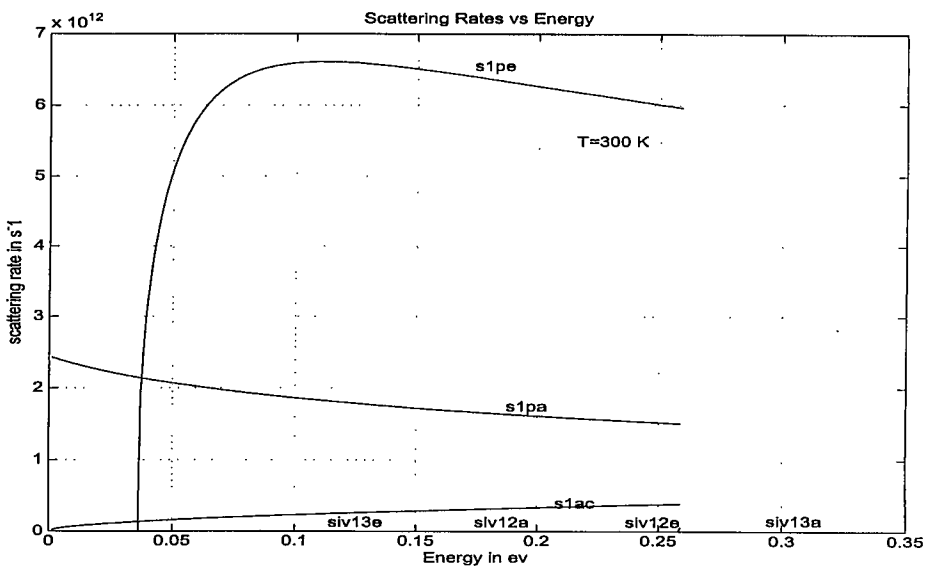

Figure 3.3 Scattering rates versus energy in valley1(Γ) for GaAs at 300K

In the above figure 'slpe' denotes the scattering rate for polar scattering process due to the emission of electrons in valley '1','slac' denotes the acoustic phonon scattering in valley'1' and siv12a' represents the inter valley scattering between valleys '1' and '2'

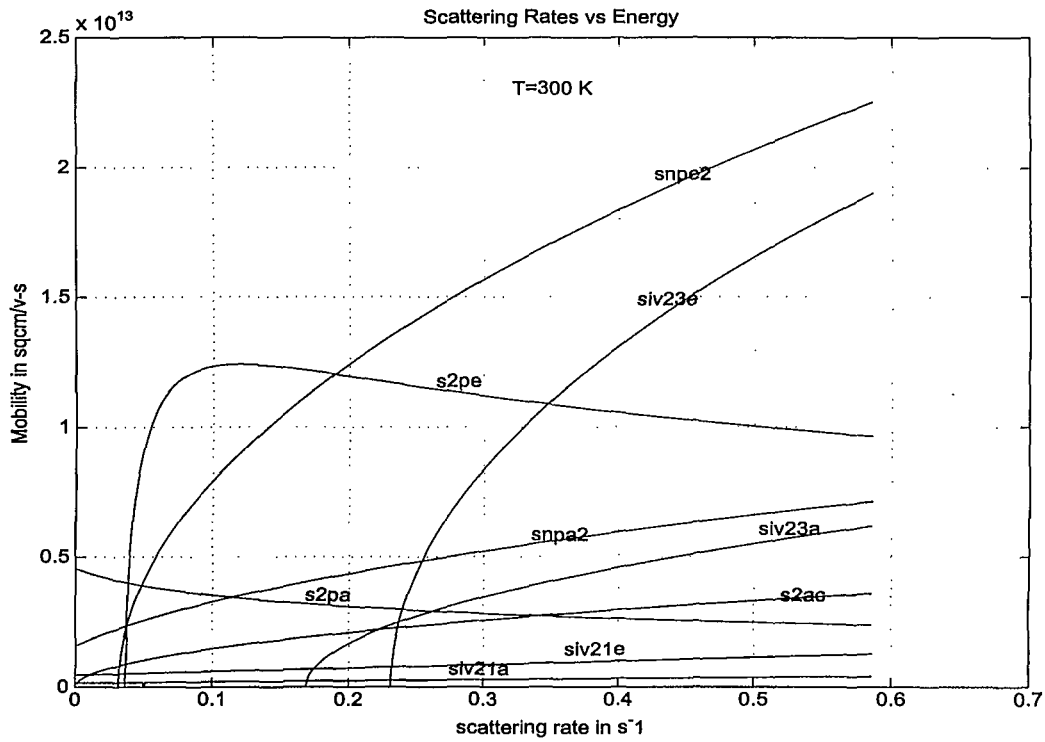

Figure 3.4 Scattering rates versus energy in valley2(L) for GaAs at 300K

due to the absorption of phonos etc.

In this figure, the various scattering mechanisms that occur in the 'L' valley are shown. The notation 'siv23a' denotes the inter valley scattering between valley '2' and'3' due to the absorption of the phonons,'siv21a' is the scattering of the electrons from valley

'2' to '1' which is also due to the absorption of phonons etc. These curves are observed at room temperature, so that the theoretical estimates could be utilized for the verification of the scattering rates in the different valleys.

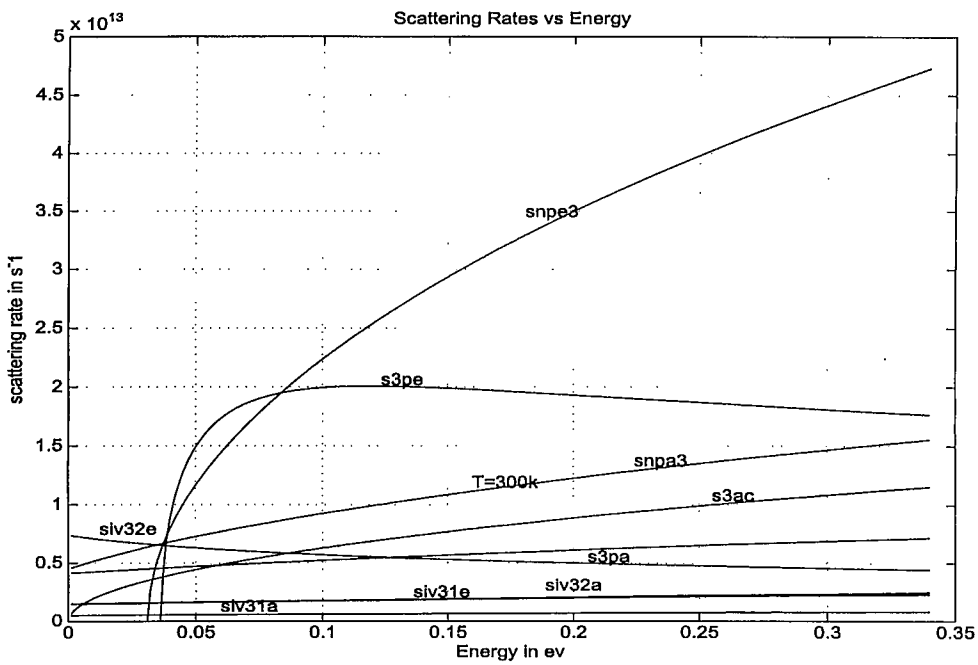

Figure 3.5 Scattering rates versus energy in valley3(X) for GaAs at 300K

Polar and non-polar optical scattering come under the optical type of lattice scattering, and represent carrier interactions with optical phonons. It is worth mentioning that lattice scattering is a broad term used for those processes that are due to atomic vibrations. Lattice vibration modes that occur at high frequencies and have associated with them a relatively higher energy on the order of several tens-of-meV are referred to as the optical phonon modes. When an electron undergoes an optical phonon scattering, it is likely to have a significant change in its momentum, since optical phonons can provide

a large energy. The optical phonon scattering rates as a function of energy are given later in this section. Optical phonon scattering is typically dominant only at higher temperatures, as the electrons need to possess that energy to emit an optical phonon. Typical optical phonon energies are: 37meV in Ge, 36 meV for GaAs, and 63 meV for Silicon.

In acoustic phonon scattering, a change in the atomic spacing produces a deformation of the lattice. This leads to a perturbation in the potential, and the process is referred to as deformation potential scattering. The magnitude of the deformation potential is proportional to the strain produced by the vibrations. Optical phonons also produce strain, and the resulting process is designated "deformation potential scattering." It is relatively important in non-polar materials such as Silicon. On the other hand, if the atoms are ionic in nature, as in GaAs, then the displacement of the atoms leads to a potential perturbation due to the charge displacements on the ions. This is called electric piezo-electric scattering if the displacements are produced by acoustic modes, or polar-optical scattering if produced by optical phonons. At low temperatures acoustic phonon processes dominate as these do not require large energy exchanges.

Inter-valley scattering involves the transitions between two valleys. A large amount of momentum is exchanged in this process. The strength of the polar interactions is inversely proportional to the momentum, and hence, this process is relatively weak for this transition. The wave vector 'q' of the phonons causing the inter-valley transitions is roughly equal to the distance between the minima of the initial and final valleys in the

Brillouin zone. This fixes 'q' for a given pair of valleys, and so these transitions are constant for a given phonon mode. This also suggests that inter-valley scattering can well be treated in terms of the deformation theory. The scattering rate versus energy for different materials is also included here as shown in Fig 3.6 [24]. The figure helps provide an understanding of magnitudes of the scattering mechanisms at 300 K in a more concise manner.

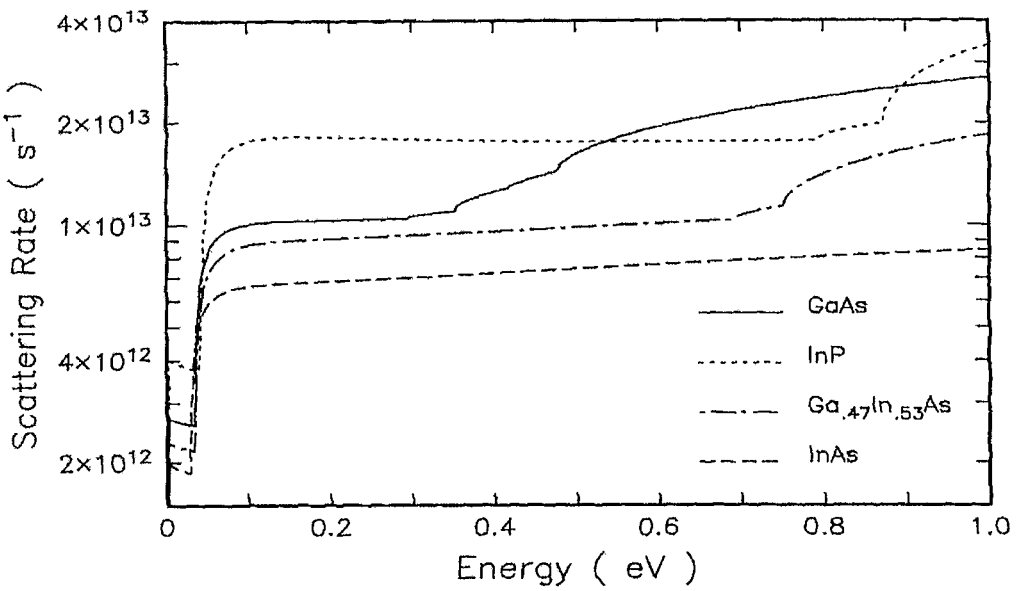

Figure 3.6 Scattering rate versus energy for various materials [24]

Like the other scattering mechanisms, ionized impurity scattering is also not affected by the applied external field. It is elastic in nature given the large mass of the interacting ion. The source for this ionized impurity is a screened Coulomb potential. Screening is necessary since mobile charges always tend to move in response to a potential. This movement can lead either to an accumulation or depletion of mobile charge in the vicinity of the scattering potential. The net effect is a reduction of the Coulomb potential,

which is represented as effectively being screened. Mathematically, in the absence of such screening, a pure Coulomb potential which is inversely proportional to the distance, and distorts a plane electron wave at all distances, would produce an infinite scattering cross section.

3.5 Simulation Results and Characteristics of GaAs

3.5.1 Theory of GaAs

The material for which the Monte Carlo simulations are carried out in this work is Gallium Antimonide (GaSb). However, GaSb is a relatively new material, and not much experimental data is available. Hence, it becomes difficult to gauge the validity and accuracy of the theoretical results and predictions by simply applying the MC technique to GaSb. A more careful evaluation is required, in order to assess the correctness. Towards this end, MC simulations were first performed for GaAs material. The GaAs material system has been well studied, and so experimental data is readily available for comparison with the MC results. A good comparison for GaAs would help establish the validity of the current MC simulation scheme and its numerical implementation.

Electron transport transients in GaAs are a typical example of its transport characteristics. These transients are generally dominated by either a net transfer of electrons from the conduction band valley to the L or X valleys, or alternatively by a net transfer from the higher energy valleys back to the Γ valley. For the present discussion and validity check, the Γ valley is taken to be in an initial equilibrium state. On the sudden application of an electric field, these electrons are accelerated to high velocity

states in the Γ-valley and then scatter to the lower velocity states in the L or X valleys. A typical Monte Carlo simulation calculation of this type is shown in the graph of fig 3.7.

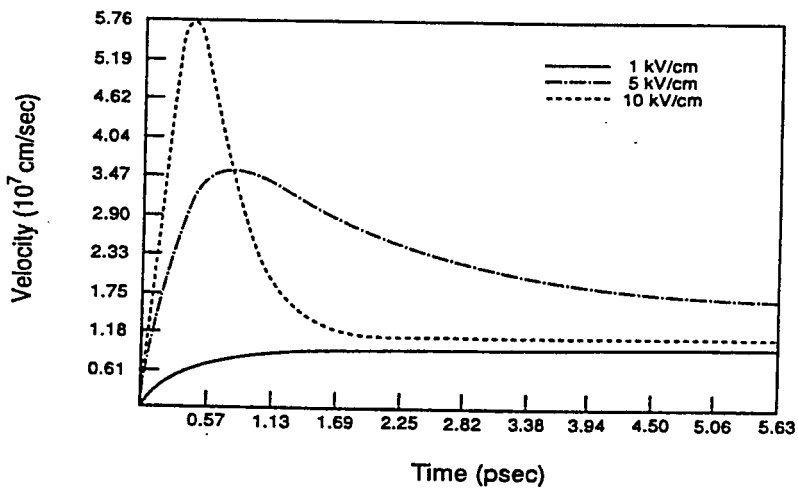

Figure 3.7 Transient electron velocities versus time for different fields assuming an initial Maxwellian distribution.

The physical origin, well known as the Jones Rees effect [32], is illustrated above. When carriers enter the Γ valley from the L-valley they can take either a positive or a

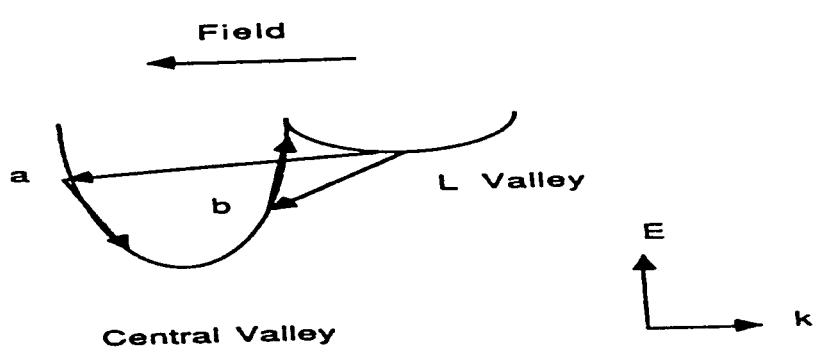

Figure 3.8 Schematic of Jones Rees effect

negative velocity. This difference due to the polarity of charges is, however, due to the presence of the electric field. Electrons entering with a positive velocity gain energy from the field and therefore, are ballistically placed into states above the inter-valley scattering threshold. Electrons entering the Γvalley with a negative velocity, however, lose energy to the field and are ballistically placed into states below the inter-valley threshold. The result is that the transfer from L to Γ valley predominantly uses the negative velocity states producing the transient dip. This Jones Rees effect is shown in the Figure 3.8. The simulation results obtained from our software code was in accordance with the above expected results and trends.

3.5.2 Monte Carlo Results For GaAs

Results for the particle transport were obtained through simulations based on the MC technique described in this chapter. A set of conduction and valence band parameters as appropriate for GaAs were used, and the values taken from available electric field, from the literature [18,33]. Specifically, the transient response of carriers in a uniform photo generated by a short laser pulse was taken as the test case.

The Monte Carlo program used for the simulation included carrier generation from the heavy-hole, light-hole, and split –off bands. In the MC simulation run, the transient velocities versus time for different field values at various temperatures were computed. The results obtained are presented in Fig. 3.9, and are seen to compare well with

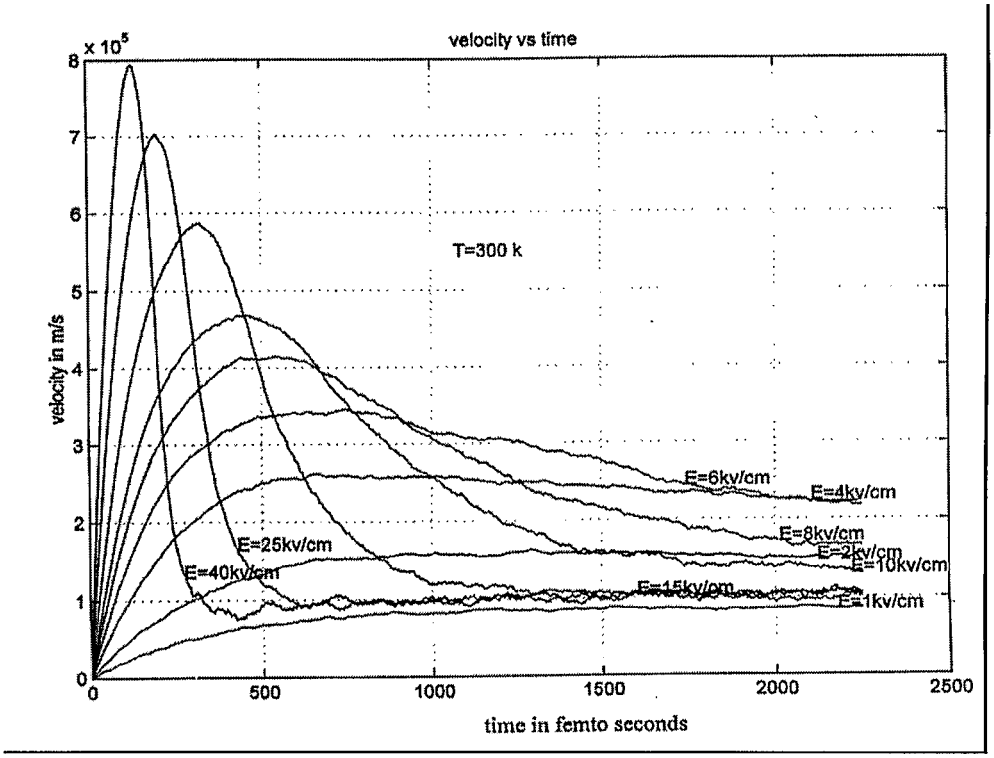

Figure 3.9 Velocity versus time for various fields at room temperature

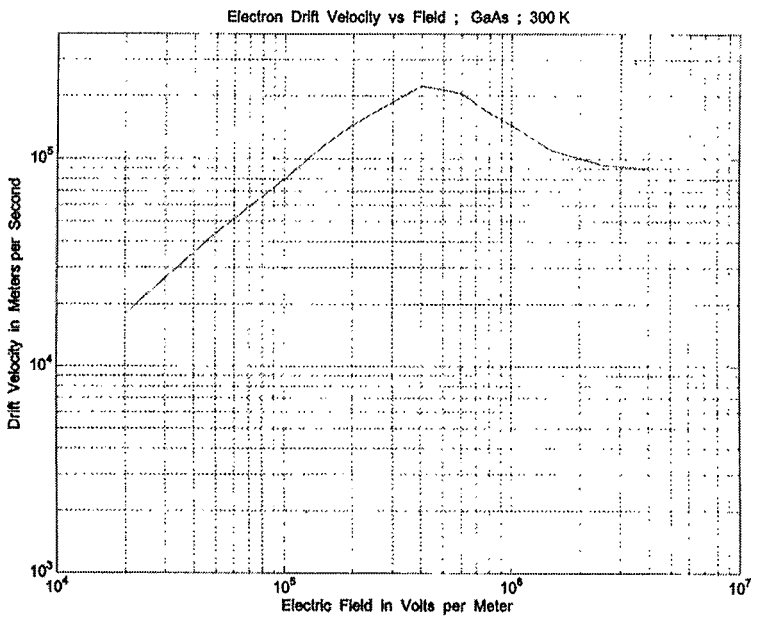

Figure 3.10 Velocity versus electric field at room temperature for GaAs

those obtained from Sze [18].A general conclusion from the curves obtained in the

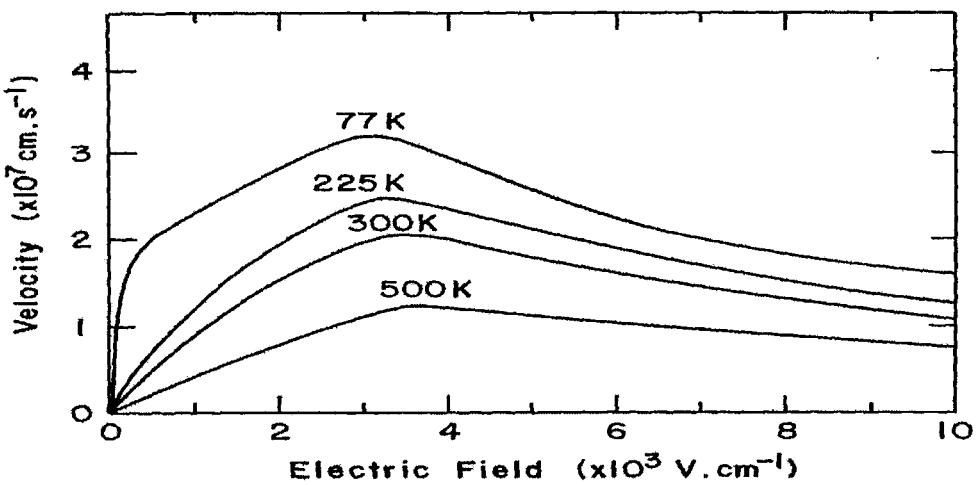

Figure 3.11 Velocity versus field characteristics for electrons as a function of e-field for various temperatures

simulation run is that the electric field is allowed to increase, the electrons in the lower valley get excited to the normally unoccupied upper valleys. This results in a differential negative resistance, and is a well known effect first discussed by Ridley [34]. Next, steady state values obtained from the simulation data at various fields were used to generate the dc velocity-field (V-E) curves. These V-E characteristics, shown in Fig. 3.10, again compare very well with previously published reports [35]. The velocity versus field curves for electrons in lightly doped GaAs for various temperatures [18] is shown in Fig. 3.11. From this figure, it is evident that for GaAs a wide range of differential negative mobility exists for fields above 3 kV/cm. Also, in figure 3.9 the

high field velocity approaches at 8x 10^5 cm/s at room temperature. This match provides further evidence of the validity of the present MC approach and the accuracy of its numerical implementation.

Electron Mobility Behavior

Carrier mobility basically depends on and is controlled by the scattering mechanisms. At room temperature, the scattering processes that dominate are both the ionized impurity scattering and the phonon scattering. At low temperatures, however, phonon scattering becomes negligible as the lattice vibrations weaken in the absence of thermal energy. So at low temperatures, the ionized impurity scattering and deformation potential scattering dominate.

The curves for drift mobility of GaAs as a function of temperature obtained from the Monte Carlo simulation is shown as in figure 3.12. A comparison of these curves

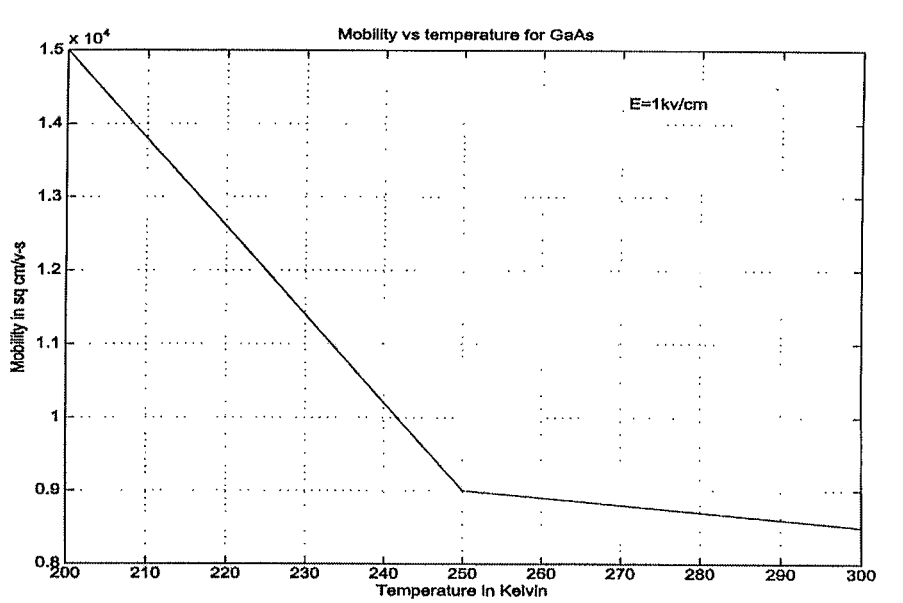

Figure 3.12 Mobility versus temperature for GaAs obtained from MC simulation

could be made with the theoretical data shown in figure 3.13 [16].

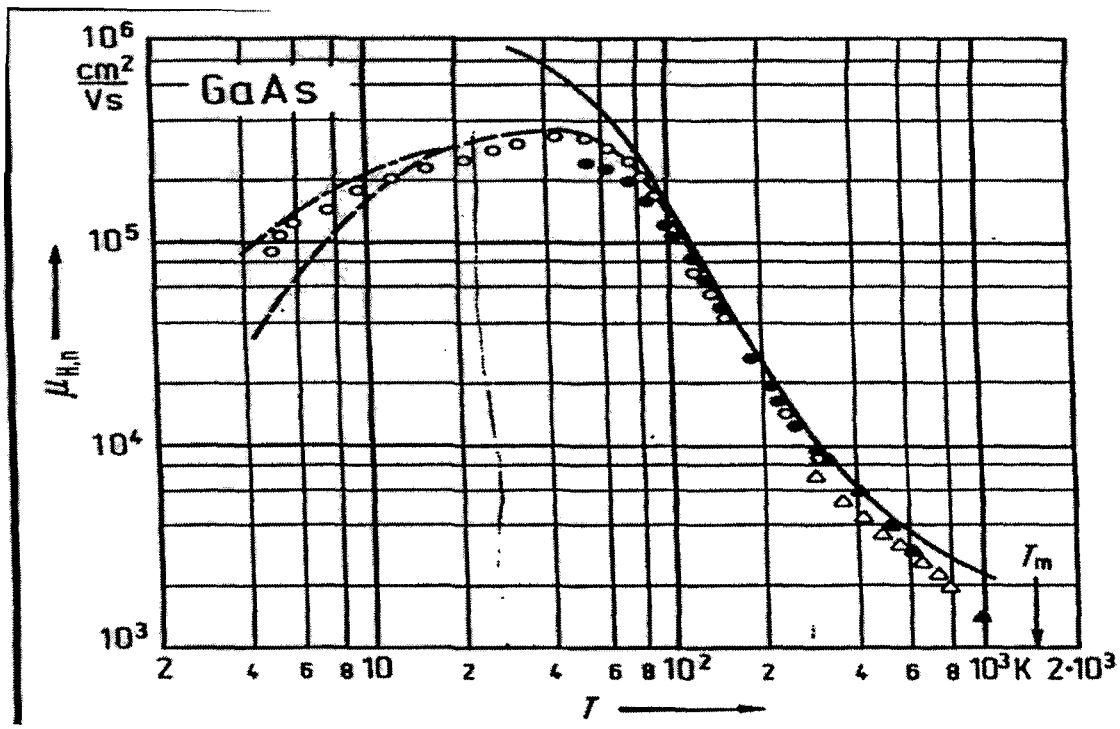

Figure 3.13 GaAs mobility of electrons versus temperature published data [16]

The mobility curves obtained from the Monte Carlo simulation shows that the motion of the electrons decreases as the temperature increases. This can be easily stated from the fact that as temperature increases the electrons encounter scattering mechanisms more rapidly, because they acquire more energy. The values obtained agree perfectly with those available in the early-published results for temperatures 200,250 and 300 K. This is shown in figure 3.13.

This section as a whole describes the Monte Carlo simulation technique implemented for the purpose of particle motion (electrons) in GaSb and the results are compared with

the same as obtained for GaAs. The various curves shown in this section as above clearly presents the dependence of the various parameters on one another. The verification of these results so obtained is achieved by the comparison relative to the theoretical estimates.

CHAPTER IV

SIMULATION RESULTS

4.1 Introduction

This chapter summarizes all the Monte Carlo simulation results obtained in this thesis research. As described in the previous chapter, the particle-based, Monte Carlo scheme has been used to simulate the electrical transport inside the Gallium Antimonide material. The motion of electrons and holes inside the GaSb material was followed as a result, and the various scattering processes that the particles undergo during their movement within the semiconductor were comprehensively considered. The results obtained have been compared with those that exist for Gallium Arsenide. The main goal of this research work is to explore the advantages of GaSb for advanced high-speed applications, as compared to GaAs material that has been investigated and is in common use at the present time. The GaAs material is currently used in photo-mixer and photodetector applications based on the concepts outlined in chapter 2. However, as stated previously, this material has potential drawbacks associated with the low mobility of holes. Hence, a numerical evaluation of GaSb as carried out and discussed in detail in this chapter is a worthwhile and meaningful exercise. At the end of this chapter, the available experimental data is briefly discussed and compared with some of the Monte Carlo results obtained. The simulation predictions are shown to match available experimental data very well. It is also shown that the GaSb material has a quantitative edge over GaAs for bipolar transport applications.

4.2 Simulation Structure

The aim of the present calculations is to determine the basic transport characteristics of GaSb material to facilitate direct comparisons with GaAs, which is the primary semiconductor in use at the present time. Such a comparison would dictate and guide decisions on the suitability and feasibility of replacing the conventional GaAs material with GaSb devices in the future. At this time, therefore, there is no intention of modeling complicated device structures, but simply to ascertain the properties of bulk GaSb material. As a result, a simple rectangular simulation box taken to represent a GaSb slab has been used here. This is a typical simulation structure that is considered for particle simulation in semiconductors such as GaAs. The rectangular box is kept fixed here, though in principle, its dimensions could be varied according to the size and geometry of an actual device. Values for the spatial extent of the box assumed are specified in the program. It is assumed that a constant electric field, corresponding to an applied voltage across the two opposite faces of the box exists. Thus, simple contacts across the entire length of two parallel surfaces have been assumed. This simplifies the geometry. For more sophisticated calculations, a more complex geometry involving point/finite contacts and lateral placement could be modeled on the basis of the present basic structure. The magnitude of this electric field is a user specified variable, and can be changed to obtained a series of field-dependent predictions.

The simulation geometry is shown in Fig. 4.1. The carriers move around the box within the specified dimensions. The initial spatial distribution of carriers is specified at run time. Here, a random distribution has been used. However, in general, non-

uniformities arising from doping inhomogeneities or spatially dependent optical excitation, can be included by using a suitable distribution function. After the initial time, as the charge carriers get accelerated and move within the box, they may encounter the walls of the simulation box. For incidence on the four non-contacting surfaces, the particles are assumed to suffer specular reflection back into the box space. These are the reflecting boundaries. In the process, the particle speed remains unchanged, but their velocity is altered. On the other hand, particles incident on the two parallel end faces, which represent the contacts, they are assumed to be absorbed by the surface and reinjected from the opposite face. This maintains current continuity, and is an inelastic process since the carriers are always re-introduced from a thermalized distribution. This assumes that the injection contact (typically the cathode) is in thermal equilibrium. The distance across which the particles are allowed to drift extends from x = '0' to x = 'L' as shown in Fig. 4.1.

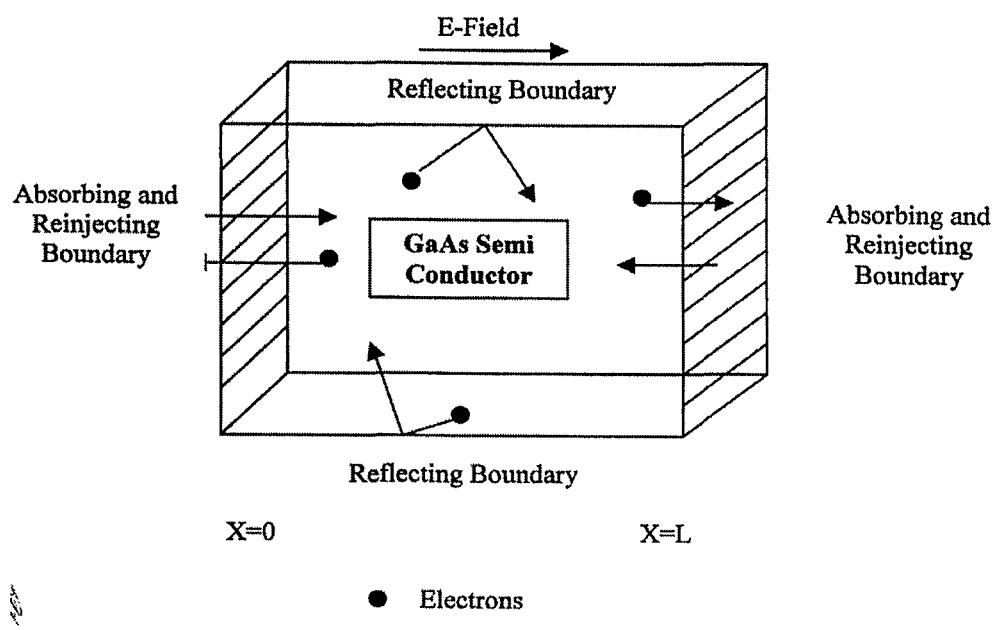

Figure 4.1 Simulation structure of the semiconductor

4.3 GaAs Results For Electrons

Results obtained from the Monte Carlo simulations for Gallium Arsenide are first described. These simulations provide a test for the numerical implementation. The GaAs was chosen since it is presently the leading contender for low-power, high-speed applications, and is also used in FET based fast switching circuits. Results for electron velocity, the relative occupancy ratio for the various valleys, the ensemble kinetic energy and the electron distribution function have been obtained and are presented in this section. Experimentally, many of the parameters such as the distribution function and particle energies cannot be probed or measured directly. Only a few parameters, such as the drift velocity can be obtained through sophisticated methods such as electro-optic sampling systems that yield time-resolved data [2]. The particle motion inside the GaAs material was simulated by means of the Monte Carlo, and the results so obtained matched the theoretical results reported in Sze [18] very well. The theoretical results from Sze are shown in figure 4.2a below. The Monte Carlo results obtained for the different fields versus their velocities is also shown below in fig 4.2b.The drift velocity initially increases monotonically with the electric field, and reaches a local maxima at a field of about 3.5 kV/cm. For higher fields, the drift velocity value subsequently starts to decrease until it reaches an eventual steady state. The velocity peaks to higher values for lower operating temperatures, but continues to exhibit the same general trends as a function of the electric fields. Physically, this implies that the particles acquire a higher mobility at lower temperatures due to decreased phonon scattering. The Monte Carlo simulation program is written in such a manner so as to compute results such as the relative valley occupancy ratio, the carrier average kinetic energy and distribution functions. The relative ratio

curves depicts the relationship between the ratio of electrons in each of the valleys to the total number of electrons in the ensemble, with respect to time. Initially, at the start of the simulation, all of the electrons are assigned to be in the lowest Γ–valley. Hence, the occupancy is 100 per cent at the start. With time, the carriers gain energy, and transcend the energy barrier into the higher-lying satellite valleys. As a result, the occupancy percentage in the Γ–valley begins decreasing with time. Finally, with increasing time, a steady state minimum value is reached. This is depicted clearly for an electric field of 1 kV at 300K in figure 4.3 below. Since, as the applied field is not large, the electrons tend to stay in the bottom-most valley. Hence, a relatively large occupancy of about 98 % is predicted. This result is in keeping with some of the published reports in the literature [5]. The kinetic energy versus time for GaAs at 300 K

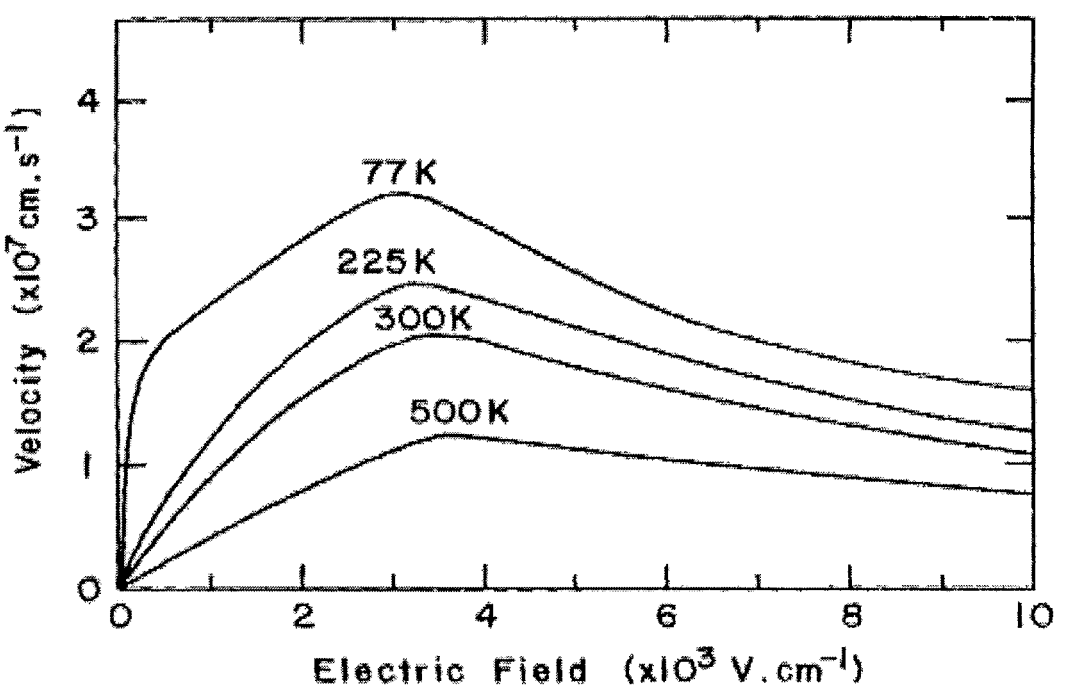

Figure 4.2a Velocity versus e- field at 300 K for GaAs from Sze[18]

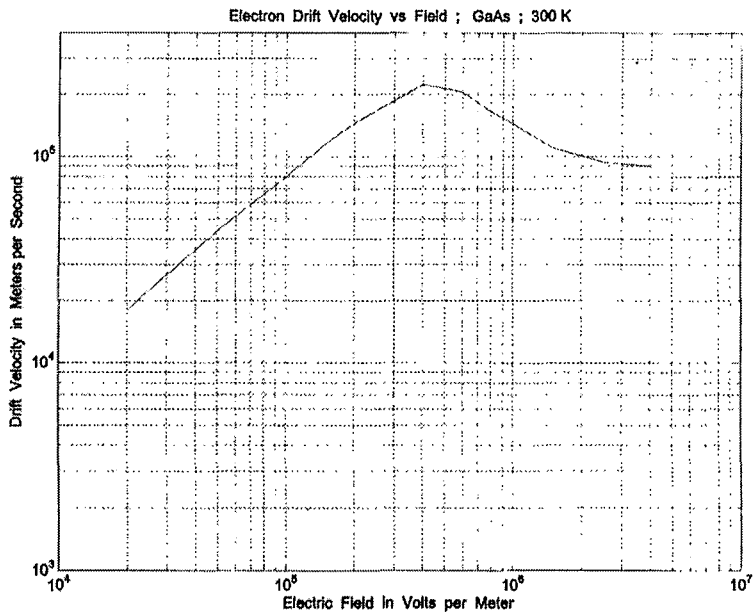

Figure 4.2b Monte-Carlo results for GaAs at 300 K

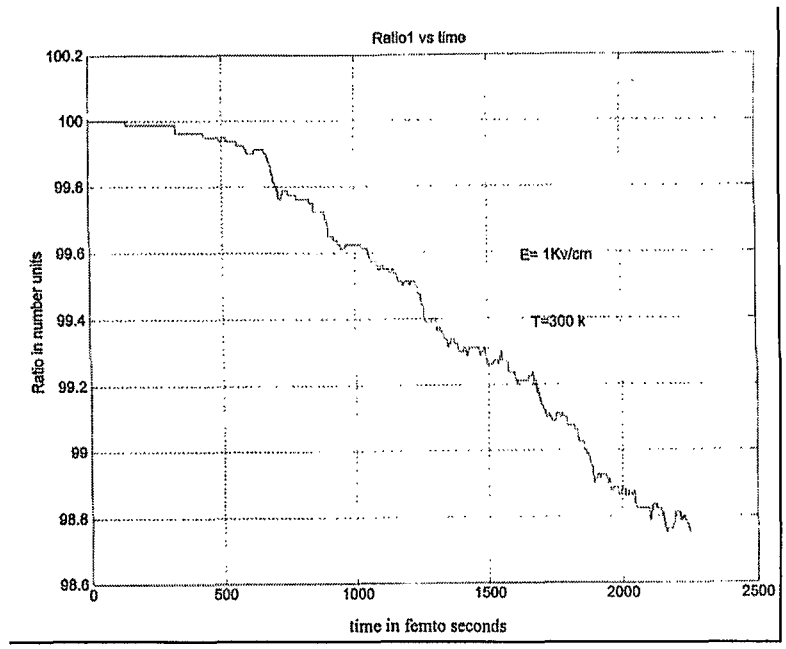

Figure 4.3 Ratio 1 versus time at 300 K for GaAs

for a voltage of 1 kV is shown in figure 4.4 below. This curve complements Fig. 4.3. It shows that with time, the electrons tend to acquire energy from the applied electric field.

A steady-state value of about 45 meV is predicted. The distribution function versus energy curve of Fig. 4.5, obtained from the Monte Carlo simulations, shows the distribution of the particles in the Γ-valleys at different energies. A relatively low electric field of 1 kV/cm was used. The function resembles the Maxwellian shape, as is expected from qualitative considerations. The curves for the satellite valleys have not been shown, since the occupancy in the higher valleys at this chosen electric field is very small. Hence, the statistical scatter in the Monte Carlo data was rather large given the finite sample size.

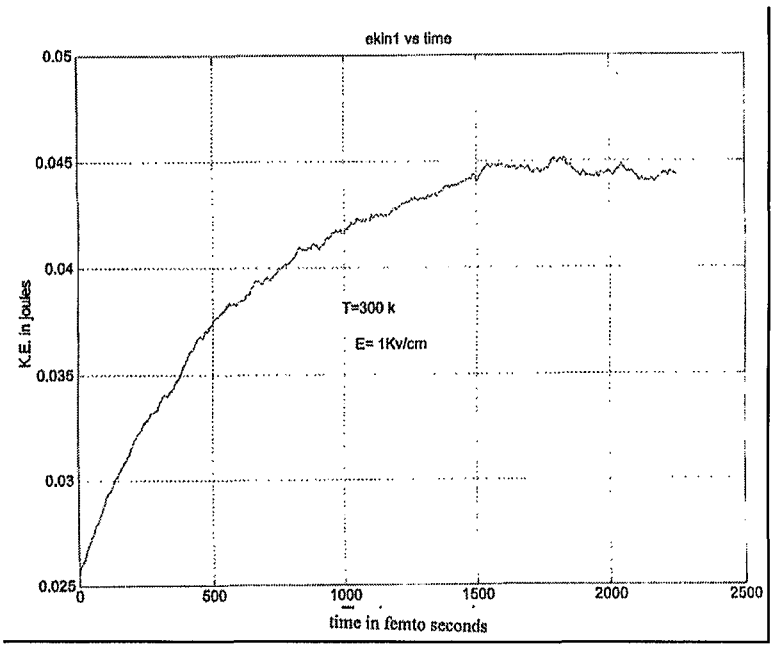

Figure 4.4 Ekin 1 versus time at 300 K for GaAs

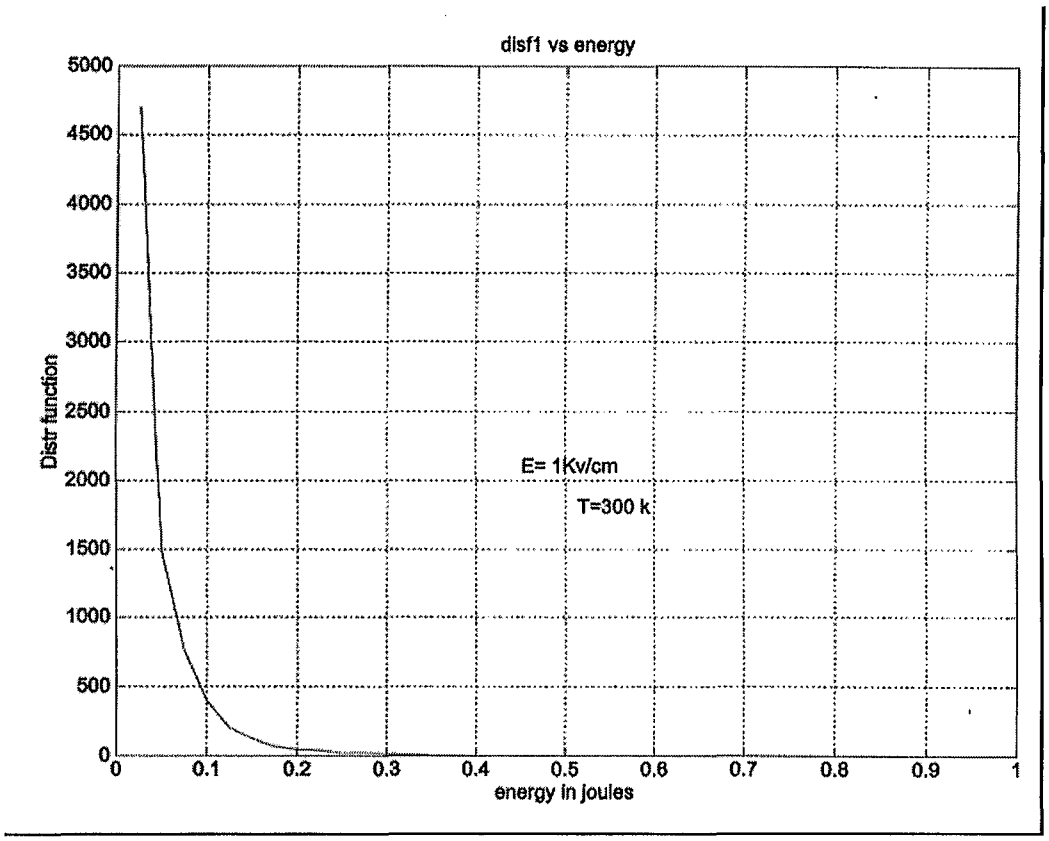

Figure 4.5 Distribution function 1 versus energy at 300 K for GaAs

The same performance measures curves for an electric field of 25 Kv/cm are shown below in figures 4.6, 4.7 and 4.8. At this high field, the electron kinetic energy of Fig. 4.6 is much higher, since the driven force is much larger. A final steady-state value of about 270 meV is predicted, an increase by about a factor of six over the low field result of Fig. 4.4. The relative Γ–valley occupancy of the electrons is shown in Fig. 4.7. As the carriers acquire much more energy from the higher applied field, more of them transcend the potential barrier and transition into the satellite valleys. As a result, a much lower

percentage (~ 13 %) are predicted to be in the Γ–valley in the steady state. Due to this small fraction, the distribution function for electrons in the Γ–valley at this high electric field, shown in Fig. 4.8, is quite jagged. The small population increases the standard deviation.

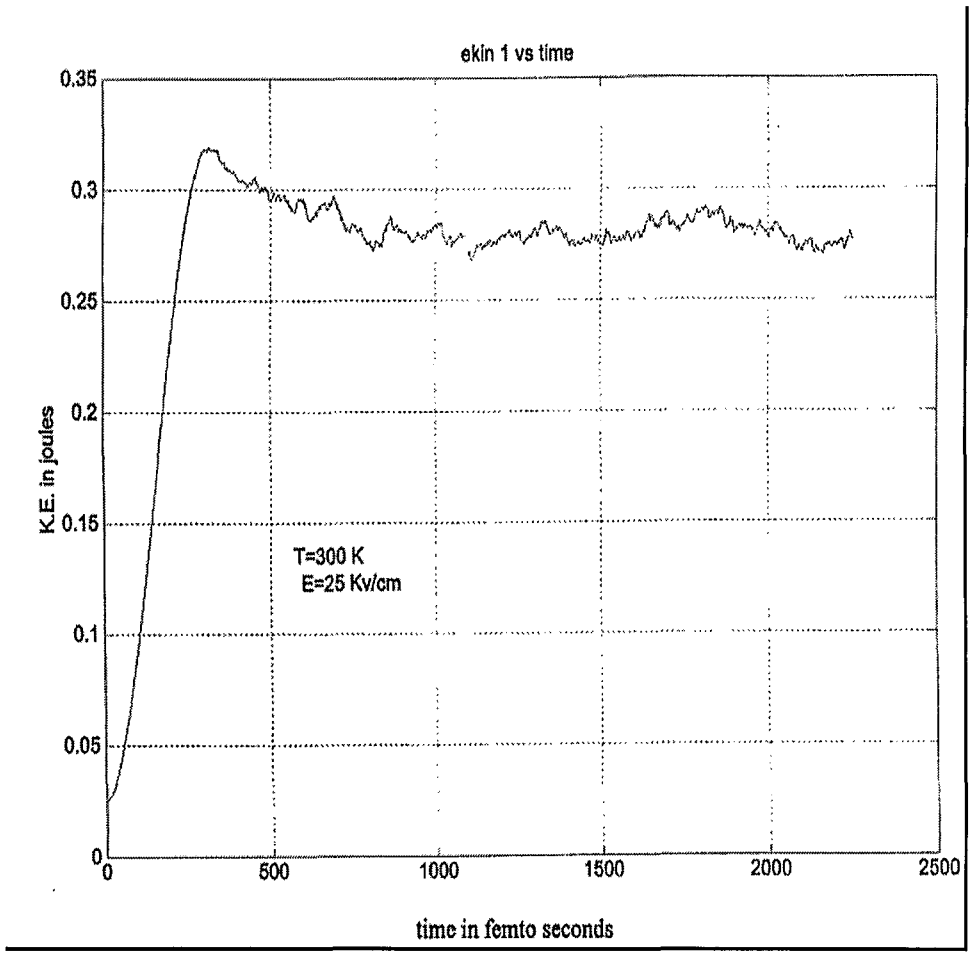

Figure 4.6 K.E. versus time at 300 K for GaAs

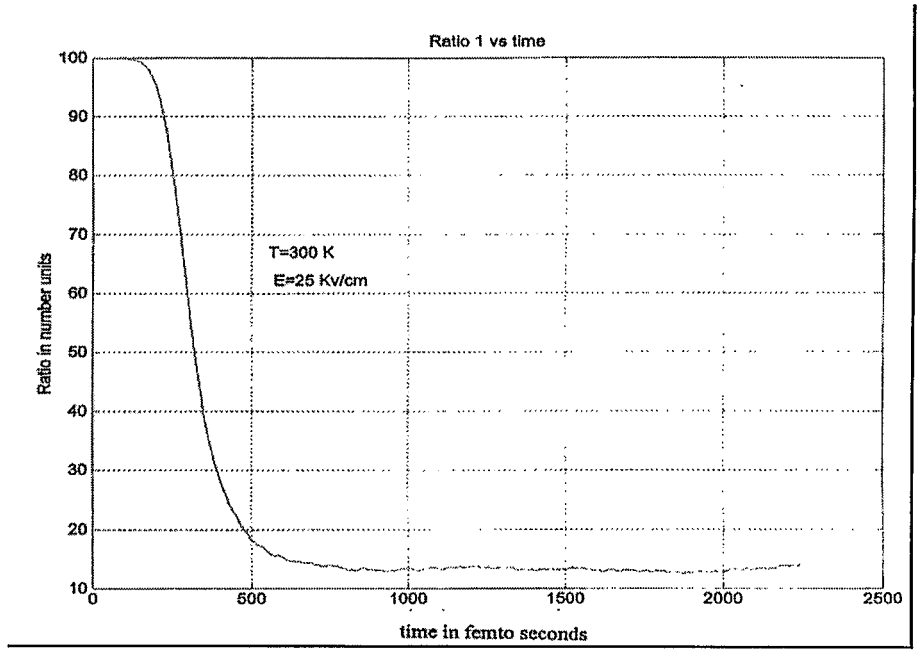

Figure 4.7 Ratio 1 versus time for GaAs at 300 K

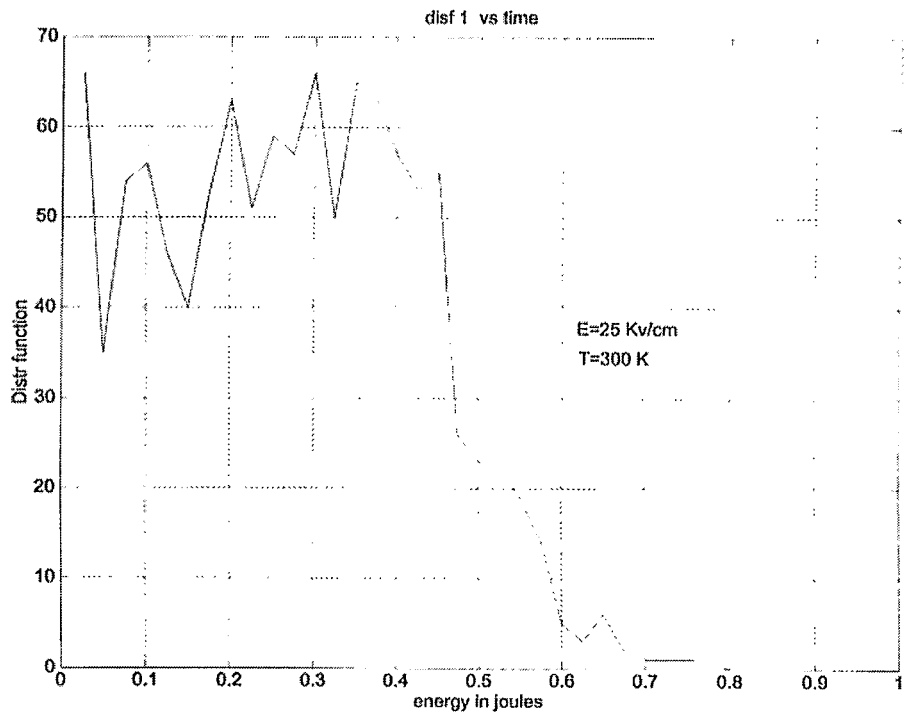

Figure 4.8 Distribution function versus energy for GaAs at 300 K

The agreement of the experimental values with the theoretical values is clearly observed from the above figures. Also, the velocity increases at a faster rate for higher electric fields, and reaches steady state in lesser time. This is due to the higher accelerating force applied. This makes the material well suited for low power, high-speed applications.

4.4 GaSb Results For Electrons

Next, in this section, the transport results obtained for GaSb are presented and discussed. Despite the emerging technological importance of GaSb, there are not many reports on its bulk electronic transport properties. In early theoretical work, the electronic mobility was calculated as a function of temperature for high purity GaSb [36]. However, only the Γ-valley was considered, and both intervalley scattering and ionized impurity interactions were ignored. A single valley model presents a potentially serious error, even at low electric fields, given the small intervalley energy separation and the large disparity between the Γ- and L-valley effective masses. More recently, electron mobility calculations based on the relaxation time approximation were reported based on a two-valley model [37]. However, as is well known, this approximation is not rigorous in that it does not provide a detailed account of the energy dependent scattering rates, nor an adequate description of the distribution functions within various bands.

Here both the electron mobility and drift velocity calculations have been performed for GaSb based on the Monte Carlo (MC) approach. A three-valley model has been used, and anisotropy effects included by explicitly incorporating all equivalent L- and X-valleys. Most of the material parameters were chosen from the literature [17,18].

However, effective mass values were taken from the recent cyclotron resonance data of Arimoto et al. [13], while the Γ-L valley deformation potential $D_{\Gamma\text{-}L}$ was set to 6 x 10^{10} eV cm^{-1} in keeping with recent pump-probe experimental data [17]. Data on the wavelength dependent effective masses was used to extract the non-parabolicity [13]. Intervalley scattering was treated using a single effective deformation potential, assumed to take account of the various symmetry-allowed phonon processes [38]. The Monte Carlo model included electron intravalley interactions with acoustic modes via the deformation potential, polar optical phonon processes, and impurity ion scattering. The Γ-L and L-L transitions occur under both the longitudinal acoustic (LA) and longitudinal optical (LO) modes [4.10]. However, following Lee and Woolley [40], a value of 23.76 meV which lies between the LA and LO frequencies, has been used here. Parameters used here for the GaSb model are given in Chapter 2. Some of the data values shown have been taken from the recent publication by Arimoto et al. [41].

The salient features of this numerical study include: (i) Low field electron mobility calculations at temperatures of 77 K and 300 K as a function of doping density. (ii) Direct comparisons with available experimental data. Unlike previous work [42], it is shown here that X-valley does not play a role in determining the mobility. (iii) Predictions of the velocity-field characteristics at the operating temperatures of 200 K and 300 K. (iv) Evaluation of the intervalley population as a function of applied field and operating temperatures.

Results of the electron mobility obtained from the Monte Carlo simulations are shown in Fig. 4.9. Operating temperatures of 77 K and 300 K were chosen, based on the availability of experimental data for comparison. Our predictions at 300 K compare especially well with those of Chen and Cho [42], and are reasonably close to the values obtained by other researchers [4, 43] as well. In our simulations, the occupancy of the highest X-valley, though not shown here, was found to be zero for all the simulation points. This is in contrast to an early report which invoked X-valley transfer to match the GaSb electron mobility with available experimental data [41]. A maximum room temperature mobility of about 5500 $cm^2\ V^{-1}s^{-1}$ is predicted. This is not too substantially lower than the GaAs value of about 7900 $cm^2\ V^{-1}s^{-1}$ [44]. This result, from a transport standpoint appears to be quite encouraging, and suggests that GaSb could have potential utility in high-speed applications. It indicates that despite the small Γ-L valley separation leading to the presence of electrons in the high mass L-valley of GaSb, the disparity in overall mobilities between the two materials would be relatively small. This occurs because the Γ-valley effective mass for GaSb is only 0.04 m_o as compared to the much higher 0.063 m_o value for GaAs. This partially helps offset the intervalley effect. Based on the above reasoning, one might perhaps expect the low temperature GaSb mobility to exceed that of GaAs as the intervalley transfer was virtually eliminated. This, however, is not the case as shown in the upper 77 K curve in Fig. 4.9. The maximum mobility predicted for GaSb is about 68,000 $cm^2\ V^{-1}s^{-1}$ which is lower than the 200,000 $cm^2\ V^{-1}s^{-1}$ value for GaAs [45].

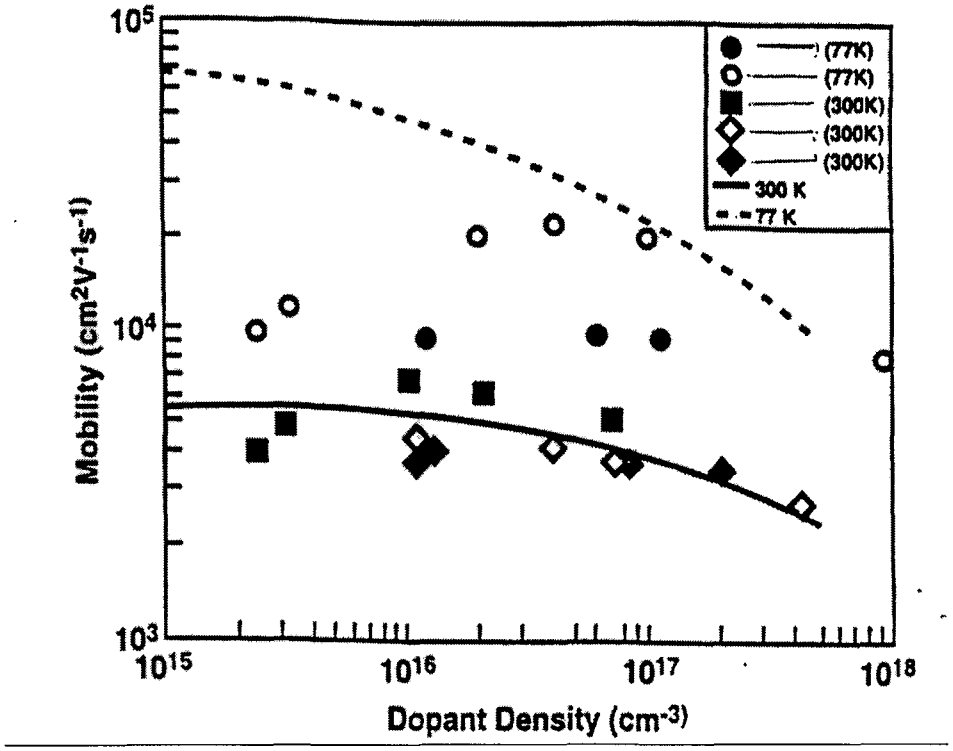

Figure 4.9 Mobility versus dopant density for GaSb electrons

The following factors contribute to this smaller low-temperature mobility: (A) Higher acoustic deformation potential for GaSb which leads to enhanced acoustic phonon scattering; (B) A lower acoustic velocity which has the same effect; (C) Lower optical phonon energy quanta, which substantially increases the phonon emission rates in GaSb. This is especially important at lower temperatures, since a significantly higher fraction of electrons would then be above the phonon emission threshold, and could participate in this scattering event.

The upper curve at 77 K exhibits a larger slope due to the dominance of ionized impurity scattering relative to the other mechanisms at low temperatures. Due to this

dominance, the overall scattering rate increases monotonically with density. However, at 300 K, the effect of the ionized impurity process is partially masked by the phonon interactions, and so the effect is not as significant. Screening of the polar interactions also contributes towards reducing the mobility declines. A quick comment about the experimental data is perhaps warranted. In general, the data appears to be lower than the theoretical predictions obtained here. This is probably due to the existence of additional processes which have been neglected here. For example, some degree of compensation is known to exist in actual samples. This is likely to increase the contribution of impurity scattering as shown by us previously [46]. Furthermore, the presence of internal strain within the GaSb films grown by MBE on underlying substrates could effectively reduce the mobility. Under these conditions, piezoelectric scattering not considered here could begin to play a role. It might also be mentioned that one of the measured data exhibits a local maxima [4]. This trend is not predicted here, and has not been observed in other measurements either.

Simulation results of the field-dependent electron drift velocity are presented and discussed next. The temporal development of the drift velocities is shown in Fig. 4.10 at 300 K for a range of electric fields. As with GaAs, an overshoot effect associated with L-valley transfer is evident. The peak velocity increases with the applied field, while the final steady state values are seen to be lower at the higher field values. This gives rise to a negative differential velocity-field characteristic as shown later. Compared with the GaAs transient behavior [33], the results here for GaSb show a larger peak drift velocity at the high electric fields. This suggests that GaSb would be a good candidate for high

speed applications utilizing scaled down device geometries. The corresponding curves for an operating temperature of 200 K are given in Fig. 4.11. The general behavior and trends are similar to those of Fig.4.11. However, due to the lower phonon scattering at 200 K, the velocity values are all higher.

Based on the temporal velocity curves of Figs. 4.10 and 4.11, the field dependent steady state drift velocity characteristics were obtained. The curves are shown in Fig. 4.12. Peak velocities of about 2.5 x 10^4 m s^{-1} and 7.4 x 10^4 m s^{-1} are predicted at 300 K

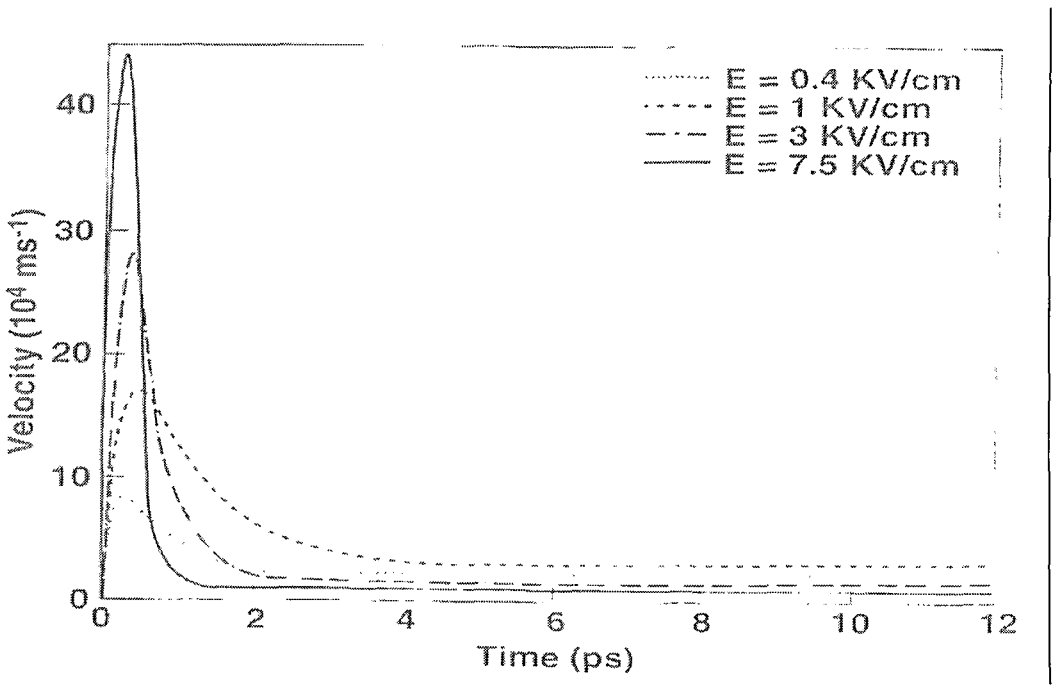

Figure 4.10 Electron drift velocity versus time at 300 K

and 200 K, respectively. As compared to GaAs, these values are significantly lower, and occur at fields much smaller than the 4 kV cm^{-1} threshold value typical of GaAs.

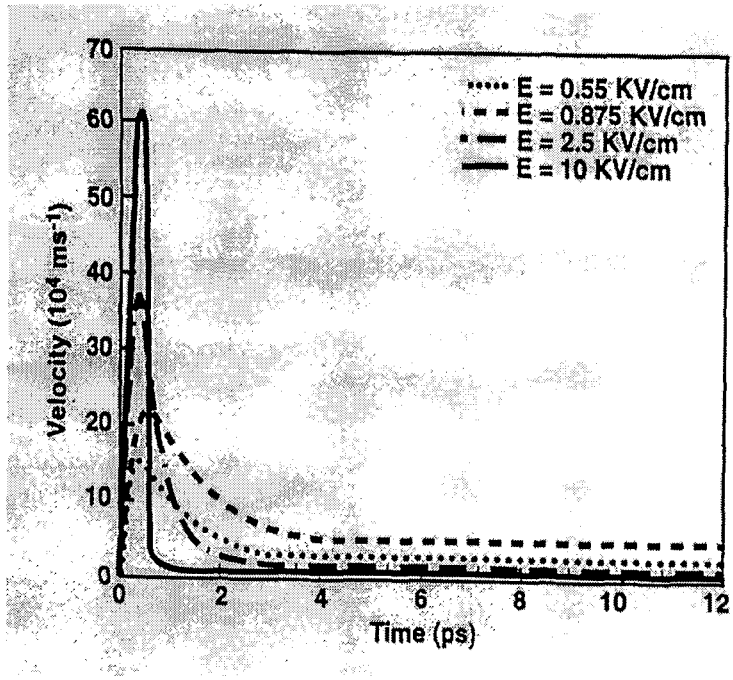

Figure 4.11 Electron drift velocity versus time at 200 K.

The characteristics clearly indicate that this material can only be a serious candidate for transient applications or in scaled down devices. Its steady state transport behavior is inferior to GaAs. Also, the GaSb velocity-field curves obtained here are flatter because the electrons are able to populate the satellite L-valleys for all of the electric field values chosen in Fig. 4.12. Hence, no sudden transition from a single to multi-valley transport occurs, and the fraction of carriers in the L-valley is always greater than zero in this chosen range of electric fields. Very roughly, the overall drift velocity v_{dr} (E) can be expressed in terms of the constituent Γ- and L-valley mobilities μ_Γ and μ_L as: v_{dr} (E) = E [$\mu_\Gamma F_\Gamma$ (E) + $\mu_L F_L$ (E)] , where F_Γ (E) and F_L (E) are the field-dependent fractional carrier occupancies in the â- and L- valleys. Hence, the local maxima corresponds to an

operating point at which the decreasing rate of F_Γ (E) with field just offsets the increases due to E and F_L (E).

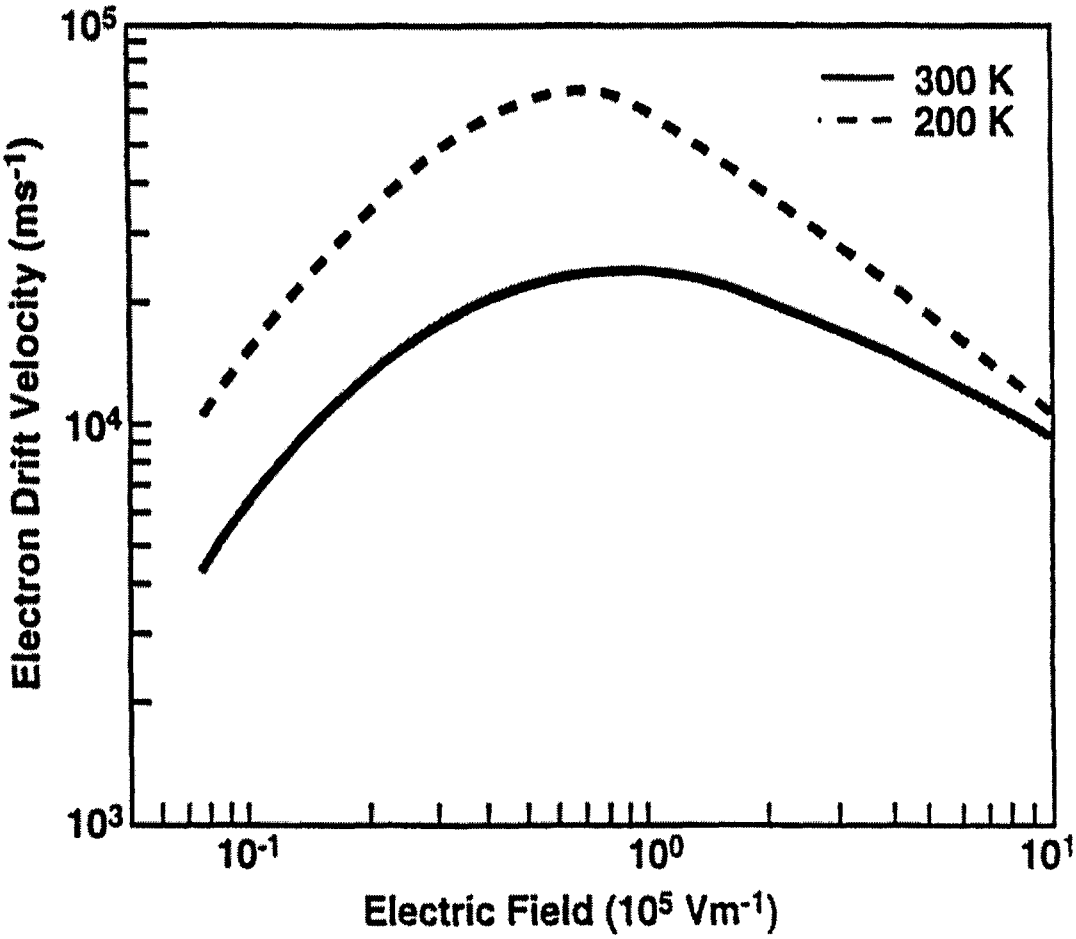

Figure 4.12 Drift velocity versus e-field at 200 K and 300 K for GaSb electrons

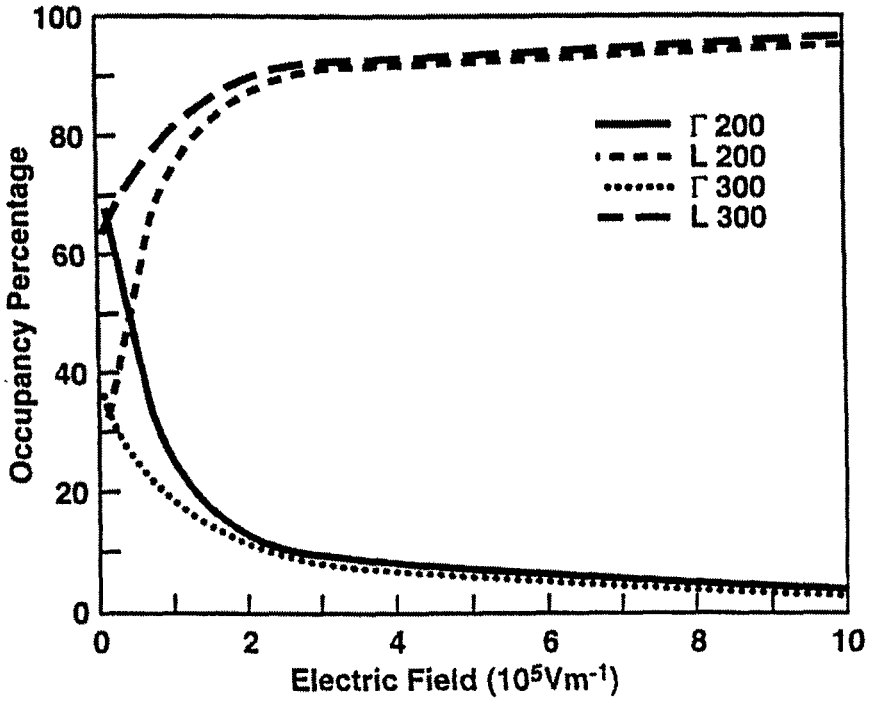

Fig 4.13 Time dependent evolution of valley 1 and 2 occupancies at 300 K

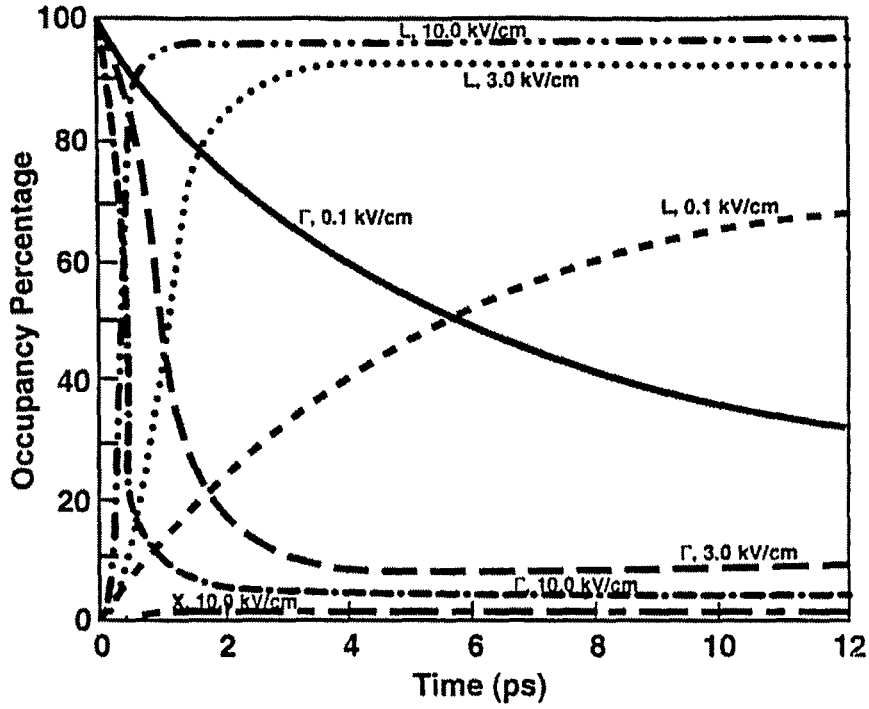

Figure 4.14 Monte-Carlo results of steady state valley occupancies at 300 K and 200 k for GaSb

The valley occupancy transient characteristics at 300 K for a few sample applied electric fields are shown in Fig. 4.13. As expected, the general trend is towards a faster onset of L-valley transfer with increasing field, with correspondingly higher fractional occupancies F_L (E). The results also indicate that the X-valley occupancy is nearly zero for low fields. The value for an electric field as high as 10 kV/cm is barely 1 percent. Thus, this result clearly negates the hypothesis of X-valley electron transport as predicted in early work on GaSb [42]. The steady state occupancies at 300 K and 200 K are given in Fig. 4.14 as a function of the applied field. As expected, the curves for F_Γ (E) are lower at the higher temperature due to phonon assisted intervalley transfers.

4.5 GaAs Results for Holes

In order to provide appropriate comparisons of the hole transport characteristics, the results for GaAs were first obtained, and are discussed in this section. In the following sections, results for GaSb will be presented, and compared to the corresponding behavior in GaAs. The time dependent velocity curves for GaAs at 200 K, for various values of the applied electric fields are shown in Fig 4.15. The same curves are shown for the room temperature also in Fig 4.16. The peak velocity for the highest field of 25 kV/cm is the largest. In fact, there is a monotonic increase in peak velocity with the electric field. The steady state values also differ for each field, but unlike electrons, the values are higher the larger the value of the electric field. This suggests positive differential velocity

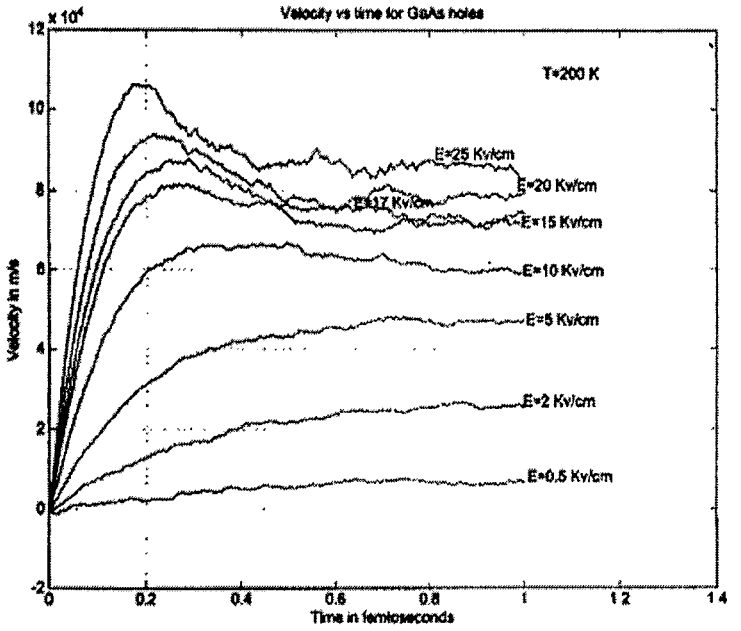

Fig 4.15 Velocity versus time at 200 K for GaAs

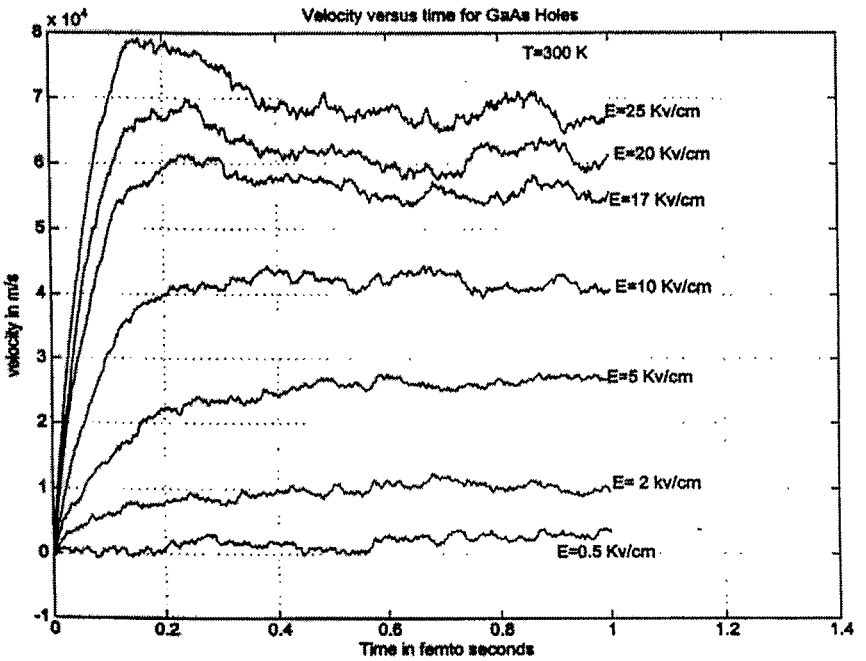

Fig 4.16 Velocity versus time a 300 K for GaAs

characteristics, and hence, a lack of potential system instabilities. The velocity versus time characteristics at operating temperatures of 250 K were also obtained. However, these are not shown here for the following reasons: (1) First, the present emphasis is on GaSb, and so excessive details pertinent to another material system such as GaAs, are not as important or germane. (2) Moreover, the curves were similar to those shown for 300 K and 200 K, with no significant or anomalous features worth discussing. The results (at both 200 K and 250 K) simply showed that the peak velocity values at various fields were larger as compared to those at 300 K. The positive differential velocity characteristics were still maintained though. The simulation results for performance measures like ratio and average energy for both the valleys are also observed. Figures 4.17 and 4.18 represent the time dependence of the various performance measures at 300 K.

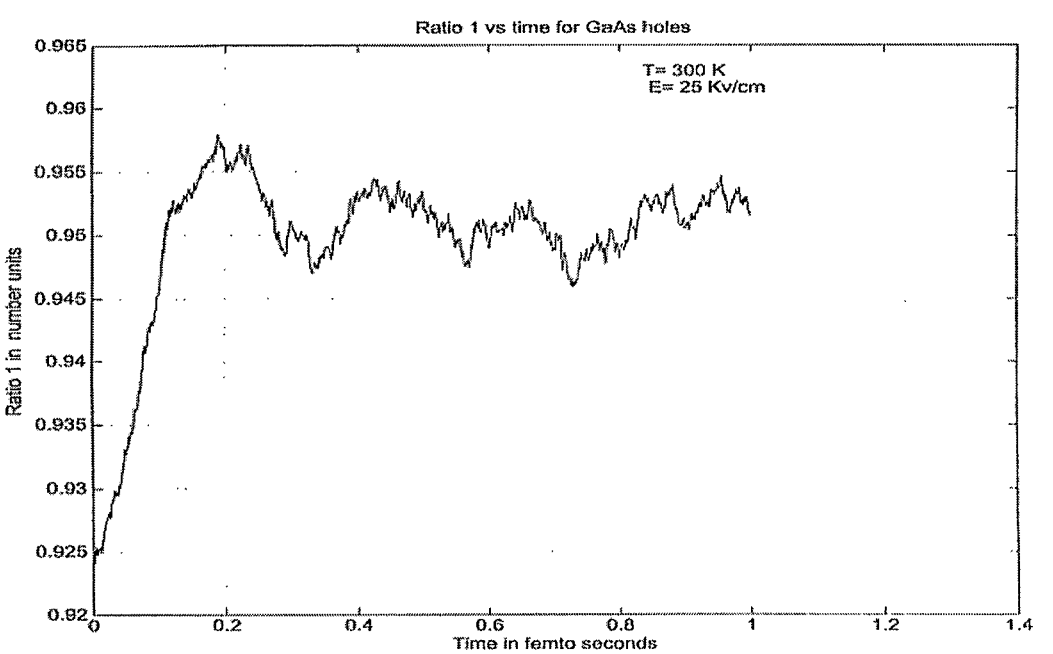

Figure 4.17 Ratio 1 versus time for GaAs holes at 300 K

Figure 4.17 shows the fractional ratio of the heavy holes. The overall numbers are quite high, and reveal that the occupancy of the heavy-hole band is substantial even at the large applied field of 25 kV/cm. The initial jump in the occupancy represents the transitions of light holes to the heavy-hole band. These process results from the higher heavy-hole density of states, which facilitates the net inter valley-scattering. Finally, a steady state value is predicted.

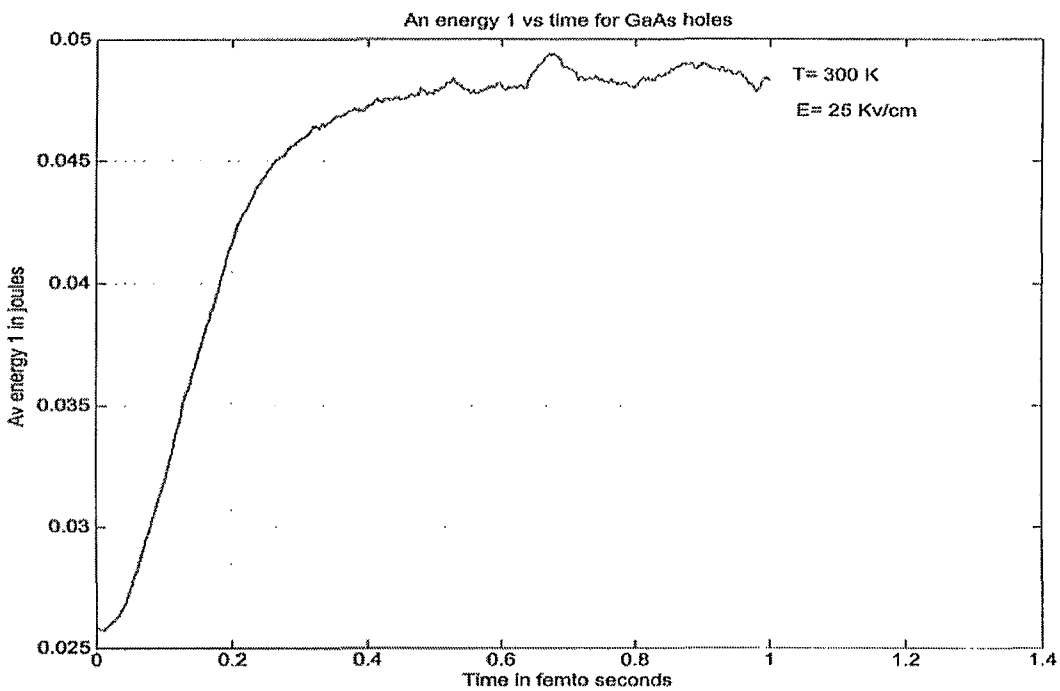

Fig 4.18 Average energy 1 versus time for GaAs at 300 K

The average energy in the heavy-hole band increases as the holes accelerate during the first several hundred femto-seconds. The net balance between energy gain from the field and the loss to phonons sets up a final steady state value.

4.6 GaSb Results for Holes

Despite the emerging technological importance of GaSb, there are not many reports on its bulk transport properties. For example, there are calculations of hole transport in bulk GaSb. Details of the velocity-field characteristics, transient response, and effects of warping all remain to be analyzed. Though hole transport in polar III-V materials has generally been reviewed by Kranzer [47], Wiley [4.8], and Costato et al. [49], the only application to GaSb was the low-field mobility calculations based on the relaxation time approximation [50-52]. In this section, we focus on the high-field transport of holes in GaSb, obtain both the transient and steady response characteristics, and make suitable comparisons with GaAs.

The present study is guided, in part, by a need to ascertain whether material other than GaAs could be used to suitably enhance the electrical response of bipolar bulk devices. Though the electronic transport properties of GaAs are clearly superior due to its low Γ-valley effective mass, its hole response is significantly slower. This can be a potential bottleneck in situations where both electrons and holes contribute to the device conduction. For example, in high-speed bulk photodetectors, it has been shown that hole transport can severely limit the device frequency response [53,54,16]. Based purely on a smaller heavy hole effective mass with respect to GaAs, one can expect the GaSb material to be a serious contender for photodetectors. In particular, faster transient behavior would greatly augment the transit speed and decrease the carrier flush-out times. This could conceivably eliminate the need for recombination-dominated material such as LT-GaAs, which suffer from thermal management problems.

For Monte Carlo calculations, a two-band model has been used to take account of both the heavy- and light-holes. Most of the material parameters were chosen from the literature [50,51,18], and the actual values used are given in table 2 in chapter 2. The main difference between electron and hole transport in polar semiconductors that influences their transport properties is the degenerate valence band structure and the symmetry properties of the wave functions. This, as originally discussed by Wiley [48], gives rise to anisotropic overlap factors that differ from unity, and a net enhancement of hole mobilities. The Monte Carlo treatment of hole scattering was based on a model for hole transport in polar materials described in detail by Costato et al. [49]. It included hole interactions with acoustic modes via the deformation potential mechanism, polar optical phonon processes, and non-polar optical scattering.

Polar-optical scattering has an important affect on the hole transport as was first pointed out by Kranzer [47]. Both the interband and intraband scattering events were taken into consideration due to the close proximity of the heavy- and light-hole bands. It is expected that light-holes would make frequent transitions into the heavy-hole band due to its larger density of states. Interband scattering was treated using a single effective deformation potential, assumed to take account of the various symmetry-allowed phonon processes. Finally, impurity scattering was ignored in this treatment for several reasons. First, neglecting impurity scattering would naturally yield a theoretical upper limit. Next, since the present aim is to ascertain the suitability of bulk GaSb material for high-speed photodetectors, there would be no intentional impurities present under these conditions.

Such devices would employ near-intrinsic material to lower noise, and decrease impurity scattering related speed reductions.

Warping of the valence bands has been included based on a nonquadratic model proposed for III-V compounds including GaSb [55,56]. Accordingly, the relation between the carrier kinetic energy E(k) and the wavevector "k" is given as :

$$E(k) = [\ 2/(2m_0)\ ]\ \{Ak^2 + [\ B^2 k^4 + C^2 (k_x^2 k_y^2 + k_x^2 k_y^2 + k_x^2 k_y^2\ )\ ]^{0.5}\ \}\ , \qquad (4.1)$$

where m_0 is the free electron mass, while k_x , k_y , and k_z are the Cartesian components of the wavevector. In equation (1), A, B , and C are fixed warping constants, which have been determined to have the values of A = 11 + 0.6, B = 6 + 1.5, and C = 11 + 4 for GaSb [57]. Strictly, the above equation needs to be modified slightly through the inclusion of a linear term in "k" as shown by Dresselhaus [58]. This arises due to the lack of inversion symmetry in zinc-blende structures. However, this correction mainly affects the low energy region of the bandstructure. As demonstrated on the basis of galvanomagnetic data by Robert et al. [59], it is mainly relevant at low temperatures. At room temperature, which has been considered throughout the present simulations, the effects are negligible and the nonquadratic model of equation (1) is roughly accurate. Furthermore, since the emphasis here is on high field transport, and not low field mobilities, the carriers would be sufficiently energetic to justify neglecting the linear correction.

Results of the transient hole drift velocities obtained from Monte Carlo simulations at 300 K are shown in Fig.4.19 for different applied electric fields. The occurrence of a slight velocity overshoot is evident from the plots for fields beyond 10 kV/cm. The overshoot arises from the combined contribution of two factors. First, differences in the momentum-relaxation and energy-relaxation rates causes a transient energy build-up within the hole subsystem. This occurs because not all of the scattering processes produce substantial changes in energy. To a large extent, only the optical phonon collisions are responsible for energy relaxation, while the acoustic interactions are nearly elastic. However, all processes, contribute to momentum

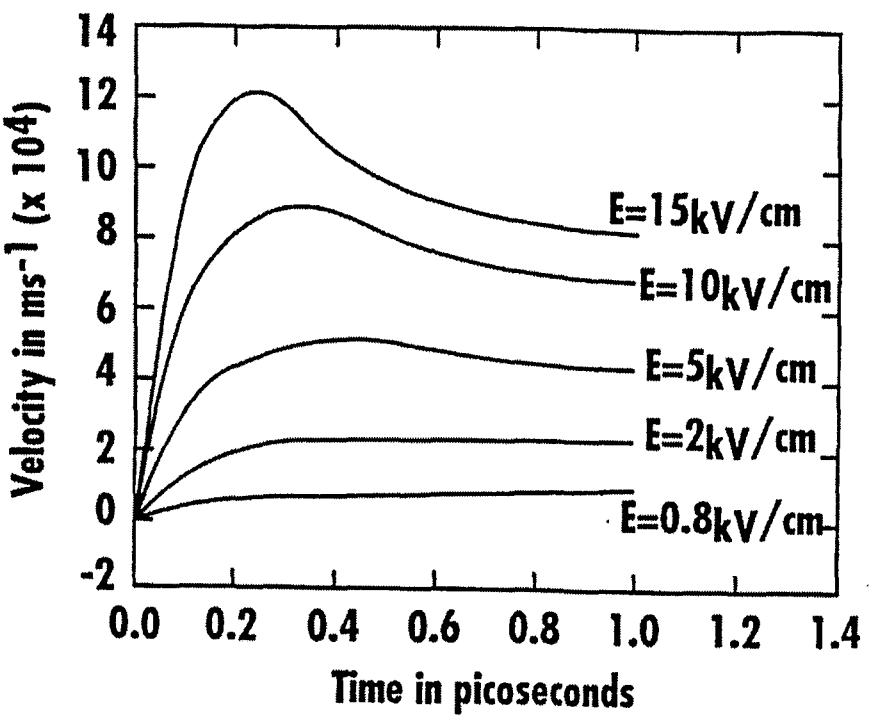

Figure 4.19 Transient hole drift velocity in GaSb from MC simulations at 300 K for various fields

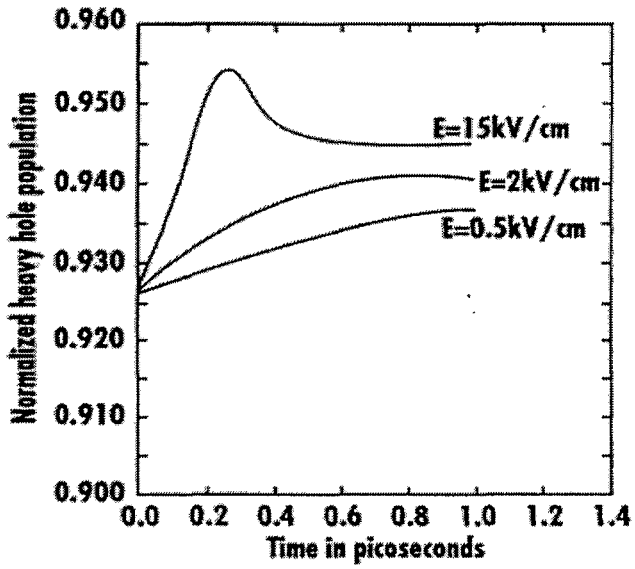

Figure 4.20 Population variation within the heavy-hole band at various electric fields.

relaxation. The net result is a transient velocity overshoot, similar to that predicted for electron transport in some indirect bandgap materials. Transient overshoot in the electron drift velocity for Silicon is a well known example, in this regard. Second, interband transfers from the light to the heavy-hole band also contribute to a transient overshoot effect. This mechanism is somewhat similar to the overshoot for electrons arising from intervalley transfer in direct bandgap materials. The transfers into the heavy-hole band can be seen from the curves of Fig. 4.20. Shown in the figure is a temporal variation of the heavy-hole population in response to different electric field step inputs. This trend can be understood in terms of the following qualitative arguments. First, the higher density of states within the heavy-hole band promotes light- to heavy-hole transitions. An additional factor is that the scattering strengths of the acoustic and non-polar optical deformation mechansims increase with phonon wave vector. This is associated with the

form of the matrix elements. Consequently, the scattering rate for transitions involving large wavevector changes is higher, as compared to those involving small wave vector variations. In particular, momentum (or wavevector) changes for the light to heavy-hole transitions are larger than those for light to light-hole intraband scattering. Consequently, under non-equilibrium conditions, the population of heavy-holes can be expected to increase at the expense of light-holes. This is borne out in Fig. 4.20. As carriers gain energy and gradually begin to surpass the phonon emission threshold under the influence of an applied field, an additional scattering channel becomes available. The net result is a gradual shift in the hole population towards the heavy-hole band. At the relatively high values of 15 kV/cm, the final steady-state occupancy is seen to be higher in Fig.4.20 than for the lower electric field. Also, a quick transient increase is predicted at the higher field due to a faster onset of interband hole transfer.

4.7 Comparison of Hole Transport Between GaSb and GaAs

The curves of Fig. 4.19 also reveal that peak velocities having values above 10^5 m s^{-1} can occur within times scales less than 0.2 ps. This, from a transport standpoint, appears to be quite encouraging, and suggests that GaSb could have potential utility in high speed detector applications employing scaled-down devices that utilize non-equilibrium transport. For comparison, results obtained for GaAs based on the published parameters [49], are shown in Fig. 4.21. The highest velocity for the 25 kV/cm field is predicted to be only about 0.8 x 10^5 m s^{-1}, much lower than that for GaSb. This weaker transport behavior is partially due to the higher effective masses for holes. The heavy- and light-hole masses for GaAs are larger than those for GaSb by factors of 1.61

(~0.45/0.28) and 1.64 (~0.082/0.05), respectively. Consequently, the hole mobilities can crudely be expected to be lower for GaAs by about 40 percent. In addition, the momentum relaxation rate between the two materials is also different. Differences in the density of states effective masses which influence the rates will tend to reduce scattering in GaSb. The following factors would also contribute :

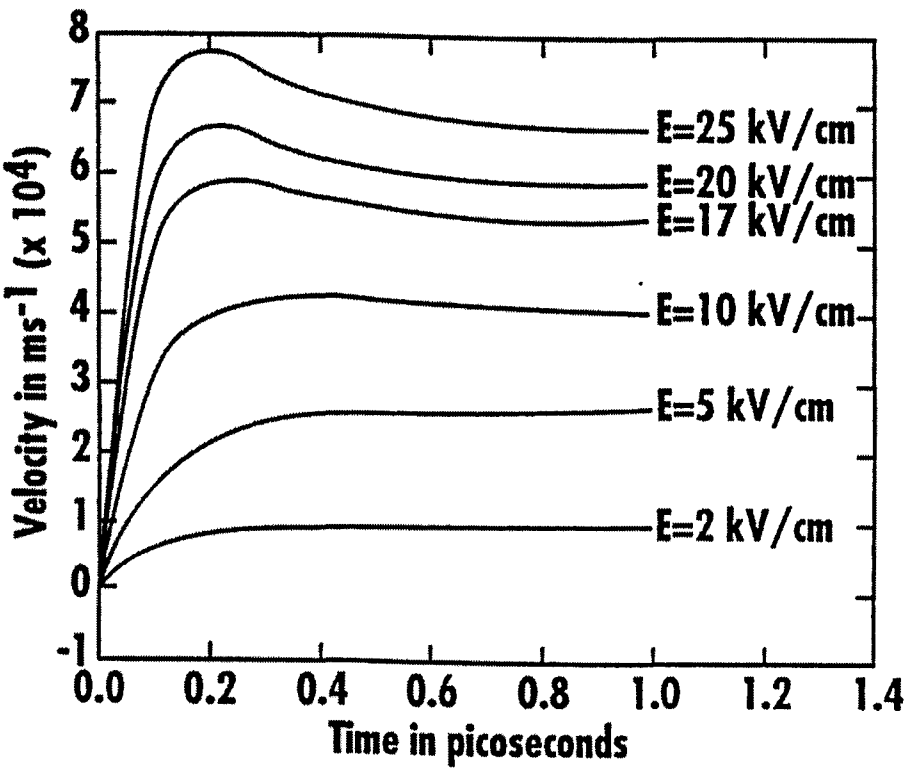

Figure 4.21 Monte-Carlo results for hole drift velocity in GaAs at 300 K for various e-fields

(A) Lower acoustic deformation potential for GaSb which leads to reduced acoustic phonon scattering. (B) A lower acoustic velocity which has the same effect. (C) Lower optical phonon energy quanta , which reduces phonon energy emissions, and leads

to increased kinetic energy for the holes. These results, also suggest that for applications to bipolar devices, the GaSb material might be a better choice over the traditional GaAs. Furthermore, the transient overshoot characteristics for GaAs in Fig. 4.21 are much lower than in GaSb. Hence, it would not be possible to take advantage of non-equilibrium hole transport in GaAs to the same extent as in GaSb.

Next, the steady state velocity-field curves were obtained based on the transient analysis presented above. The velocity v_h (E) for both GaSb and GaAs are given in Fig. 4.22 as a function of the electric field "E". The GaSb values can roughly be fit by the following curve :

$$V_h(E) = \mu E / [1 + \{\mu E / v_{sat}\}] = 0.12\, E / [1 + \{7.2727 \times 10^{-7}\, E\}]. \qquad (4.2a)$$

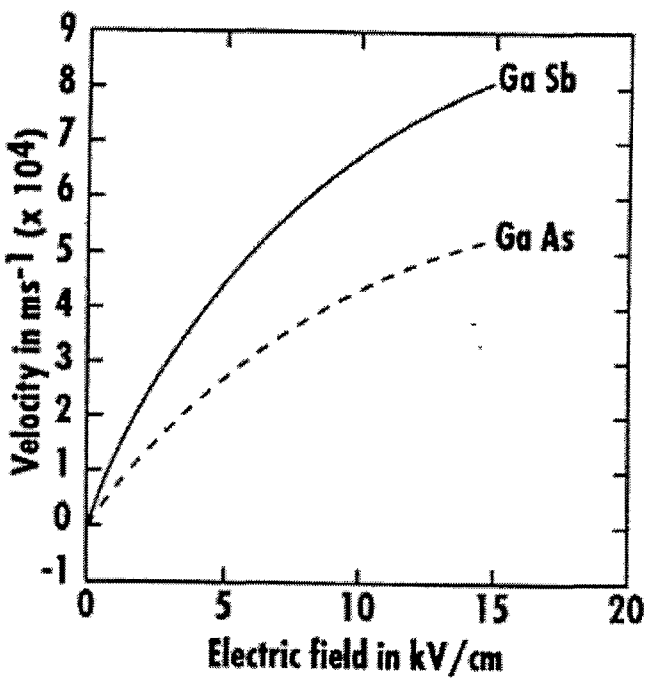

Figure 4.22 Comparison of steady state hole velocity versus e-field for GaAs and GaSb at 300K

Thus, the effective saturation velocity v_{sat} works out to be about 1.65×10^5 ms^{-1}, and with a mobility parameter of 0.12 $m^2 V^{-1} s^{-1}$. On the other hand, the corresponding expression for GaAs hole transport based on the present Monte Carlo data works out to be :

$$V_h(E) = \mu E / [1 + \{\mu E / v_{sat}\}] = 0.052\, E / [1 + \{5.2 \times 10^{-7}\, E\}] , \qquad (4.2b)$$

which translates into effective mobility and saturation velocity values of 0.12 $m^2 V^{-1} s^{-1}$ and 10^5 $m\, s^{-1}$. These magnitudes for GaAs compare quite favorably with those reportedly used in device modeling work [60].

The results obtained here show that the transient drift velocities for GaSb are higher than the corresponding values for GaAs. This arises from the lower effective masses of both the heavy- and light-holes in GaSb as compared to GaAs. The transport properties are also affected by differences in the deformation potentials and phonon quanta. The field-dependent electron velocity behavior has also been probed, and shown to be superior of GaAs. Analytical curve fits have been obtained, which should be useful for the purposes of GaSb-based device modeling. The results suggest that GaSb might be a useful material for high-speed, high-frequency optical detectors.

CHAPTER V

CONCLUSION

5.1 Conclusion Summary

A Monte Carlo simulation for the semi conductor material Gallium Antimonide, has been performed, to prove that GaSb can be used for high speed applications. The material Gallium Arsenide has already been explored by many researchers and made suitable for certain applications. In order to prove the validity of the simulation software, the program has been run for GaAs and the results obtained were compared with the theoretical results in Sze. The results matched well with each other. However, the hole properties of GaAs itself, is not so good. Due to the need for materials that can yield good transport properties for both holes and electrons, properties of GaSb were explored from the Monte Carlo results. It seems that the hole properties of GaSb agree very well, as much as for electrons, making it a better choice in high-speed applications. Numerous results have been obtained for both holes and electrons, some of which are shown in the previous chapters.

5.1.1 Summary of GaAs Results

The Monte Carlo simulation provided a solution to the particle transport mechanisms, and facilitated the evaluation of specific performance measures such as carrier drift velocity, mobility and kinetic energies, and carrier distribution functions in phase space. The various scattering processes undergone inside the material are also explored, and the results of the scattering rate versus energy are presented in chapter 3.

The shape of the curves so obtained from the simulation were seen to agree with the theoretical curve obtained for GaAs at room temperature. The drift velocities were recorded as a function of time, as well as a function of the electric field. A three-valley model was considered for the electrons and a two-valley model for the holes. The results of drift velocities for the electrons showed good and acceptable figures for high-speed photo detector applications. However, the results for GaAS holes though in agreement did not prove to be a better choice compared to the drift velocity maximum obtained for GaSb.

5.1.2 Summary of GaSb Results

5.1.2.1 GaSb Electrons

A many valley anisotropic Monte Carlo model was considered for the simulation of electrons in the semiconductor material. The model that has been used incorporates electron intravalley interactions with acoustic modes via deformation potential, polar optical phonon processes, and ionized impurity ion scattering. The occupancy of the highest valley was found to be zero at all points. The ionized impurity scattering dominates at lower temperatures in the order of 77 K, which offsets the mobility, and it was found to be high at higher temperatures, because polar optical scattering dominates in that region. At 200 K the general behavior of the electrons looks similar, but due to lower phonon scattering, the velocity values seem to be higher. However, the steady state transport behavior is inferior compared to that of GaAs. The GaSb velocity field curves appear to be flatter because of the population of the L valley for all the electric fields. In the increasing velocity regime, GaSb curves are positioned

higher compared to GaAs. This is shown in chapter 4. This suggests GaSb as a good choice for high-speed optical photo detectors.

5.1.2.2 GaSb Holes

A two-valley model has been used to incorporate light- and heavy-hole band to investigate the hole properties in GaSb. Electron mobility calculations have generally relied on a variety of approximations, such as the single valley model, or the relaxation time approximation. There is only a single Monte Carlo study that provided electronic mobility simulations based on a many valley model, and which yielded both steady state and transient drift velocity characteristics. Hole transport properties being superior, becomes more important in situations where both electrons and holes contribute to the device conduction. The light-holes were seen to make frequent transitions into the heavy-hole band, owing to their larger density of states. There is a slight velocity overshoot evident for fields beyond 10 Kv/cm. The difference in the mass of the holes is one of the reasons for this. The peak velocities have values higher than 10^5 m/s within time scales of 0.2 ps. This appears to be a little encouraging since GaSb can be used for high speed applications, owing to its high potential utility. The highest velocity for 25 Kv/cm is predicted to be lesser for GaAs compared to that of GaSb. This is because of the higher hole effective mass of GaAs. The above reasons hold GaSb promising for several research applications. Currently there are no reports for the GaSb hole properties in comparison with GaAs. This research work provides rigorous calculations from the Monte Carlo methods. The deformation potentials and phonon quanta also

affect the transport properties. The results suggest that the GaSb material can be used for high speed, high frequency applications.

5.2 Suggestions for Future Work

This work has accomplished the tasks of exploring the properties and transport mechanisms of the semiconductor material Gallium Antimonide. The basic study of the material has been made in this work, in order to justify the material as good or bad. There are many more things to be worked on about this material to gain knowledge about its depth and its performance for extended applications. Some areas which were not concentrated or given emphasis are:

(1) The valence bands are degenerate, and its coupling effects are not considered. The coupling of the bands induces changes in the scattering mechanisms and other properties.

(2) The drift velocity effects are considered with respect to an applied field. This electric field is considered to be uniform, and the performance for a varying field has not been taken into account. The drift velocities are bound to act in a different manner for different positioned electrons depending on the intensity to which they experience the field.

(3) In relation to the above point, the transport mechanisms in the presence of a temperature gradient and/or a photo excitation have not been studied. The temperature has numerous effects on the performance of the material. The increase or decrease in temperature affects the mobility of the carriers, runaway effect due to lattice heating and various other transport properties.

(4) The steady state behavior of GaSb is not very good compared to that of GaAs. This high field property has to be examined more to improve this problem.

(5) When the field values are increased, the carriers start moving in opposite directions, depending on the polarity. This creates an internal field due to the polarization that opposes the applied field. The effect is called the Polarization effect, which is not accounted for at any point in this work.

(6) This work explores the basic characteristics of the material with respect to certain applied electric fields. The results seem convincing for using GaSb in various applications. This material can be used in photo detector applications. Some processing problems may arise which need to be explored. It may also prove to be better compared to GaAs MSM photo detectors owing to its betterment in its obtained performance measures.

It is seen from the above facts that this work has just set a starting stone for this material, GaSb. If the incomplete work is accomplished in near future, there are great chances to gain deeper knowledge about GaSb and leave a history behind for various other specific research areas.

REFERENCES

[1] K. Victor, H.G. Roskos, and C. Waschke, J. Opt . Soc. Am. B **11**, 2470 (1994).

[2] R. P. Joshi, and J. A. McAdoo, *Applied Physics Letters*, Vol **68**, No.14, 1 April (1996).

[3] A. G. Milnes and A.Y. Polyakov, *Solid State Electronics* **36**, 803 (1993).

[4] G. W. Turner, S. J. Eglash, and A. J. Strauss, J. Vac. Sci.Technol.B11, **864**(1993).

[5] F. Pascal , F. Delannoy, J. Bougnot, L. Gouskov, G. Bougnot, P. Grosse, and J. Electron. Mater. **19,** 187 (1990).

[6] K. F. Logenbach and W. I. Wang, *Appl.Phys.Lett,* **59**, 2427 (1991).

[7] H. Kitabayashi, T. Waho, and M. Yamamoto, *Appl.Phys.Lett*, **71**, 512 (1997).

[8] D. H. Chow,R. H. Milnes, T. C. Hasenberg, A. R. Kost, Y. H. Zhang, H. Dunlap, and L.West, *Appl .Phys. Lett*, **67**, 3700 (1995).

[9] J. Johnson , L. A. Samoska, A. C. Gossard, J. I. Mertz, M.D. Jack, G. R. Chapman, B. A. Baugmgratz, K. Kosai, and S. M. Johnson, *J.Appl.Phys* , **80**, 1116 (1996).

[10] H. Mohseni, E. Michel, J. Sandoen, M. Razeghi,W. Mitchel, and G. Brown, *Appl.Phys.Lett.* **71**, 1403 (1997).

[11] J. R. Meyer, C.A. Hoffmann, F.J. Bartoli, and L.R. Ram-Mohan, *Appl.Phys.Lett.* **67**,

2756 (1995).

[12] H. Xie, W. I. Wang, J. R. Meyer, and L.R. ram Mohan, *J.Appl.Phys.Lett.* **65,** 2048 (1994).

[13] H. Aritmoto, N. Miura, R. J. Nicholas , N. J. Mason, and P. J. Walker, Phys.Rev.B

58, 4560 (1998).

[14] N. Bouarissa, A. Zaoui, J. P. Dufuor, M. Certier, and H.Aourag, Materials Sci.Engineering **B47**, 1 (1997).

[15] T. Wang, F. Kieseling, and A.Forchel, *Phys. Rev.* **B58**, 3594 (1998) .

[16] O. Madelung, in *Physics of Group Elements and III-V compounds*, Group III, Vols. **17a** and **22a**, Landolt-Bornstein New Series (Springer-Verlag,Berlin, 1981).

[17] D. C. Smith, E. D. O'sullivan, L. Rota, A. C. Maciel , and J. F. Ryan, *Phys.Stat.Sol.* B. **204,** 110 (1997).

[18] S. M. Sze, *Modern Semi conductor Device Physics*, 1998.

[19] *Solid State Electronics* , **36**, No.6, pp. 803-818, 1993.

[20] D. K. Schroder, in *Semiconductor Material and Device Characterization,* (Wiley-Interscience, N. York, 1998).

[21] G. L. Esley, in *Coherent Raman Spectroscopy,* (Pergamon Press, Oxford, 1981).

[22] *Ion Cyclotron Resonance Spectroscopy,* edited by H. Hartmann, (Springer-Verlag, Berlin, 1978).

[23] D. V. Lang, J. Appl. Phys. **45**, 3023 (1974).

[24] S. Tiwari, in *Compound Semiconductor Devices,* (Academic Press, N. York, 1992).

[25] B. R. Nag, in *Electron Transport in Compound Semiconductors,* (Springer-Verlag, Berlin, 1980).

[26] C. Jacoboni and L. Reggiani, Rev. Mod. Phys. **55**, 645 (1983).

[27] W. Fawcett, A. D. Boardman, and S. Swain, J. Phys. Chem. Sol. **13**, 1963 (1970).

[28] C. Jacoboni and P. Lugli, in *The Monte Carlo Method for Semiconductor Device Simulation,* (Springer-Verlag, Berlin, 1989).

[29] L. L. Carter and E. D. Cashwell, in *Particle Transport Simulation With the Monte Carlo Method*, (National Technical Information Service, Washington DC, 1975).

[30] T. Kurosawa, J. Phys. Soc. Japan **21**, 424 (1966).

[31] A. D. Boardman, W. Fawcett, and H. D. Rees, Solid State Comm. **6**, 305 (1968).

[32] D. Jones and H. D. Rees, J. Phys. C **6**, 1781 (1973).

[33] S. N. Chamoun, R. P. Joshi, E. Arnold, and R. O. Grondin, J. Appl. Phys. **66**, 236 (1989).

[34] B. K. Ridley and T. B. Watkins, Proc. Phys. Soc. Lond. **78**, 293 (1961).

[35] Y. Pozhela and A. Reklaitis, Solid State Electronics **23**, 927 (1980).

[36] D. L. Rode, *Phys. Rev. B,* **2**, 1012 (1970).

[37] V. W. Chin, *Solid St. Electronics* **38**, 59 (1995).

[38] S. Zollner, S. Gopalan, and M. Cardona, *Semicond. Sci. Technol.* B**7**, 137 (1992).

[39] J. Birman, M. Lax, and R. Loudon, *Phys. Rev.* **145**, 620 (1966).

[40] H. J. Lee and J. C. Woolley, Can. *J. Phys.* **59**, 1844 (1981).

[41] J. Basinski, D. J. Demars, and J. C. Woolley, *J. Phys.* C **7**, 716 (1974).

[42] J. F. Chen and A. Y. Cho, *J. Appl. Phys.* **70**, 277 (1991).

[43] S. Subbanna, G. Tuttle, and H. Kroemer, *J. Electron. Mater.* **17**, 297 (1988).

[44] W. Walukiewicz, L. Lagowski, L. Jastrzebski, M. Lichtensteiger, and H. C. Gatos, *J. Appl. Phys* **50**, 899 (1979).

[45] L. Lin, Y. Lin, X. Zhong, Y. Zhang, and H. Li, *J. Cryst. Growth* **56**, 344 (1982).

[46] R. P. Joshi and D. K. Ferry, *Phys. Rev.* **B** 43, 9734 (1991).

[47] D. Kranzer, *Phys. Stat. Solidi* A **26**, 11 (1974) ; D. Kranzer, *J. Phys. C: Solid State Physics* **6**, 2967 (1973).

[48] J. D. Wiley, *Phys. Rev.* B **4**, 2485 (1971) ; J. D. Wiley, in *Semiconductors and Semimetals,* edited by R. K. Willardson and A. C. Beer (Academic, New York, 1975), Vol. **10**, p. 91.

[49] M. Costato, C. Jacoboni, and L. Reggiani, *Phys. Stat. Solidi* B **52**, 461 (1972); S. Bosi, C. Jacoboni, and L. Reggiani, *J. Phys.* C **12**, 1523 (1979).

[50] P. C. Mathur and S. Jain, *Phys. Rev.* B **19**, 3152 (1979).

[51] M. W. Heller and R. G. Hamerly, *J. Appl. Phys.* **57**, 4626 (1985).

[52] P. S. Dutta, V. Prasad, and H. L. Bhat, *J. Appl. Phys.* **80**, 2847 (1996).

[53] J. Kuhl, M. Klingenstein, J. Rosenzweig, C. Moglestue, and A. Axmann, *Semiconductor Science and Technology* **7**, 157 (1992) ; M. Klingenstein, J. Kuhl, J. Rosenzweig, C. Moglestue, and A. Axmann, *Appl. Phys. Lett.* **58**, 2503 (1991).

[54] S. Y. Chou, Y. Liu, W. Khalil, T. Y. Hsiang, and S. Alexandrou, *Appl. Phys. Lett.* **61**, 819 (1992).

[55] G. Dresselhaus, A. F. Kip, and C. Kittel, *Phys. Rev.* **98**, 368 (1955).

[56] B. Lax and J. G. Mavroides, *Phys. Rev.* **100**, 1650 (1955) ; J. G. Mavroides and B. Lax, *Phys. Rev.* **107**, 1530 (1957).

[57] R. A. Stradling, *Phys. Lett.* **20**, 217 (1966).

[58] G. Dresselhaus, *Phys. Rev.* **100**, 580 (1955).

[59] J. L. Robert, B. Pistoulet, D. Barjon, and A. Raymond, *J. Phys. Chem. Solids* **34**, 2221 (1973).

[60] C. D. Capps, R. A. Falk, and J. C. Adams, *J. Appl. Phys.* **74**, 6645 (1993).

VITA

Damayanthi Palaniappan was born in India, on February 13th, 1976. She started her undergraduate study in 1993 at Coimbatore, Tamilnadu, India, and obtained her bachelor of engineering degree in electronics and communication in 1997. She began her graduate study in electrical engineering in August 1998 at Old Dominion University, Norfolk, Virginia and graduated under Dr. Ravindra. P. Joshi in December 1999.